J. Fluid Mech. (2022), *vol*. 939, A29, doi:10.1017/jfm.2022.152

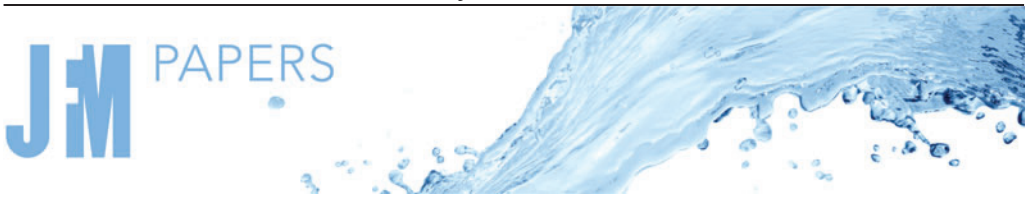

Characterising entrainment in fountains and negatively buoyant jets

L. Milton-McGurk[1],†, N. Williamson[1], S.W. Armfield[1] and M.P. Kirkpatrick[1]

[1]Department of Aerospace, Mechanical and Mechatronic Engineering, The University of Sydney, NSW 2006, Australia

(Received 8 July 2021; revised 14 December 2021; accepted 16 February 2022)

Turbulent fountain flow consists of two distinct stages, the initial 'negatively buoyant jet' (NBJ) stage, and the fully developed 'fountain' stage. The present study investigates both stages of the flow using particle image velocimetry and planar laser-induced fluorescence, over a range of source Froude numbers, $10 \lesssim Fr_o \lesssim 30$, and Reynolds numbers, $5500 \lesssim Re_o \lesssim 7700$. While the velocity and buoyancy profiles in NBJs take similar Gaussian shapes over a wide range of axial locations, this was not observed in fountains. The changing profile shape is most evident in the outer flow (OF) region, while there is a degree of similarity in the inner flow (IF). Entrainment between IF and OF is shown to depend on the local Richardson number, Ri. The fountains are found to have a negative entrainment coefficient, $\alpha < 0$, for the majority of their height, implying a net radial outflow of fluid from the IF to the OF. An alternative description of entrainment is considered, the 'decomposed top-hat' model, where the radial flow is separated into inflow and outflow components that are then estimated using the present experimental data. The inflow component was found to be proportional to the axial IF velocity, which is similar to the classical description of entrainment in pure jets/plumes, while the outflow depends on the local Ri. Entrainment in NBJs may also be described by this framework, which, despite not having an OF, is still subject to an Ri-dependent radial outflow.

Key words: buoyant jets, plumes/thermals, turbulent mixing

1. Introduction

Negatively buoyant jets (NBJs) occur when the buoyancy of a turbulent jet opposes its momentum. A vertically aligned NBJ will be decelerated by the opposing buoyancy until its momentum is reduced to zero at an 'initial rise height', z_i, where it reaches a stagnation point. For NBJs discharging from a round inlet, the flow will then reverse direction and

† Email address for correspondence: liam.milton-mcgurk@sydney.edu.au

return annularly towards the source, mixing with the opposing fluid. After some time, a quasi-steady state is reached where the flow consists of an 'inner flow' (IF), where fluid moves in the same direction in which it was discharged, and opposing annular 'outer flow' (OF), where the fluid returns towards the source. At this quasi-steady stage, the flow oscillates around its mean 'steady-state height', z_{ss}, and is referred to as a fully developed fountain. The flow during the initial rise, before z_i is reached and a return flow begins to form, is distinct from the fully developed fountain stage and will be referred to as an NBJ. Negatively buoyant jets and fountains occur in a variety of industrial applications and in nature, such as brine discharge in desalination plants (Pincince & List 1973), and explosive volcanic jets (Carazzo, Kaminski & Tait 2008; Dellino *et al.* 2014).

For high-Reynolds-number flow, the initial and steady-state heights are governed by the source Froude and Richardson numbers given by

$$Fr_o = \frac{w_o}{(-r_o b_o)^{1/2}} = \frac{1}{(-Ri_o)^{1/2}}, \tag{1.1}$$

where w_o is the initial average velocity, r_o is the source radius (for round inlets), and $b_o = g(\rho_o - \rho_a)/\rho_a$ is the source buoyancy. Here, ρ_o and ρ_a denote the densities of the source and ambient fluid, respectively, and g is the gravitational acceleration. The Reynolds number is $Re_o = w_o D/\nu_o$, where $D = 2r_o$ is the inlet diameter and ν_o is the kinematic viscosity of the source fluid.

Several previous investigations into fully developed fountains have involved taking bulk flow measurements, such as of z_i and z_{ss}, to obtain Fr_o scaling relations for the rise heights (Turner 1966; Kaye & Hunt 2006; Burridge & Hunt 2012). These have aided the classification of distinct fountain regimes by Fr_o, ranging from very weak fountains ($Fr_o \lesssim 1.0$) to highly forced fountains ($Fr_o \gtrsim 5.5$), the latter being the primary focus of the present investigation. In the high Fr_o case, the initial and steady-state heights have been shown to follow $z_{ss} = 2.46\,Fr_o$ and $z_i/z_{ss} = 1.45$ (Turner 1966; Kaye & Hunt 2006; Burridge & Hunt 2012). Other studies have sought to investigate overall entrainment and dilution in fountains, such as Burridge & Hunt (2016), who proposed scaling relations for the entrained volume flux for the different fountain classes. These previous studies, as well as the present investigation, consider Boussinesq fountains, where local variations in density are small compared to the ambient density and may be neglected except where they affect buoyancy. A more general description would be needed to describe non-Boussinesq fountains with larger density differences.

In a study by the present authors, the initial NBJ stage of the flow was investigated experimentally using two-dimensional particle image velocimetry (PIV) and planar laser-induced fluorescence (PLIF) (Milton-McGurk *et al.* 2021; Talluru *et al.* 2021). It was found that, like neutral jets and plumes, the velocity and buoyancy profiles take Gaussian shapes over a wide range of axial locations ($20 \lesssim z/D \lesssim 40$). The widths of these profiles in NBJs, however, grow at different rates. Another important difference between NBJs and neutral and positively buoyant jets/plumes is that the turbulence profiles, such as the Reynolds stress and axial fluctuations, do not scale with the mean flow. Entrainment in NBJs was also investigated in Milton-McGurk *et al.* (2021), and was found to be similar to a neutral jet near the source where the flow is more momentum-dominated. Further along the NBJ, where the flow becomes more buoyancy-dominated, the direction of 'entrainment' is reversed and there is a net radial outflow of fluid from the NBJ to the ambient.

There have also been some investigations involving local measurements of the internal velocity/scalar fields in fully developed fountains. Experimental studies by Mizushina

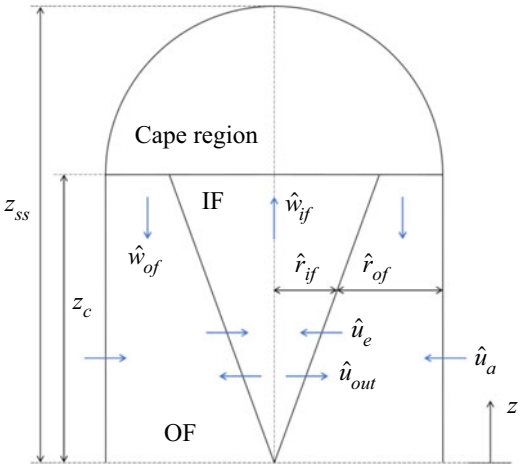

Figure 1. Schematic diagram of a fully developed fountain.

et al. (1982) and Cresswell & Szczepura (1993), and a direct numerical simulation (DNS) study by Williamson, Armfield & Lin (2011), all found that the profiles inside fountains were not self-similar. The assumption of self-similarity is common in attempts to model fountains; for example, McDougall (1981) modelled a fountain as an NBJ surrounded by an opposing OF, assumed self-similarity and used constant entrainment coefficients to describe mixing between the IF/OF layers and the ambient fluid. A schematic of a fountain described by this model is given in figure 1. Bloomfield & Kerr (2000) built upon this model and assessed alternative entrainment formulations, including relating entrainment into the IF to the relative velocity difference of the IF and OF, as well as to the IF velocity only. Both formulations under-predicted the steady-state rise height, z_{ss}, with the latter approach giving predictions closer to experiments. Hunt & Debugne (2016) developed a similar integral model, but additionally accounted for entrainment into the cap region (the top of a fountain where the fluid reverses direction). They assumed a constant entrainment coefficient that described radial flow from the OF to the IF, and obtained predictions for rise height, IF width and velocity that were in good agreement with experiments. Other experimental and numerical studies, however, have reported that the radial flow of fluid is primarily in the opposite direction, from the IF to the OF (Cresswell & Szczepura 1993; Williamson *et al.* 2011). Differences between entrainment in NBJs without a return flow, and in the fully developed fountain with the IF/OF structure, have also not been given much attention (Hunt & Debugne 2016).

While our previous work was concerned primarily with the initial NBJ stage of the flow (Milton-McGurk *et al.* 2021), the present study will extend this by using PIV and PLIF measurements to investigate the fully developed fountain stage. Since NBJs can be considered fountains without an OF, examining the differences between these two flows will allow the effect of the return flow on the IF of a fountain to be investigated. A particular focus will be placed on the IF, by considering the extent to which it can be considered an NBJ independent of the OF. There is extensive literature focused on predicting the bulk behaviour of fountains such as rise height (Turner 1966; Kaye & Hunt 2006; Burridge & Hunt 2012; Hunt & Burridge 2015), so the present study aims to investigate primarily local behaviour, including entrainment at the IF/OF boundary and how this compares to NBJs.

Time-averaged statistics for a fountain and an NBJ, both with $Fr_o = 30$, are presented in § 3, followed by a comparison of $Fr_o = 30$ and 15 fountains in § 4. The velocity decay and radial expansion of the IF are discussed in §§ 5 and 6, where a scaling for the overall fountain width is found that is consistent with previous literature (Mizushina *et al.* 1982). Entrainment in fountains and NBJs is investigated in §§ 7 and 8, with a focus on entrainment between the IF/OF regions. This is pursued by extending the approach of van Reeuwijk & Craske (2015) and Carazzo, Kaminski & Tait (2010), where a new equation for entrainment in this region as a function of the local Richardson number is derived. An alternative model of entrainment is proposed, where the net entrainment is decomposed into a constant inflow component and a locally varying outflow component in a 'decomposed top-hat' model. This builds on previous fountain models, such as those by Hunt & Debugne (2016) and Bloomfield & Kerr (2000), by allowing for non-constant entrainment between the IF and OF. The description of entrainment in these top-hat models is connected to the formulation developed by van Reeuwijk & Craske (2015) in the context of neutral and positively buoyant jets/plumes, which is based on the governing conservation equations and does not make any assumptions about profile shapes or self-similarity. Finally, in § 9, the proposed decomposed top-hat model is solved for the fully developed fountains and compared to the present experimental data.

2. Experiments

With the same experimental set-up as used in Milton-McGurk *et al.* (2020, 2021), PIV and PLIF measurements are obtained for the NBJ and fountain stages of the flow. This involves using four pco.2000 CCD cameras, and an additional IDS uEye camera, capturing images simultaneously with pulses from a 532 nm Nd:YAG laser. Two pco cameras were used to obtained images for the PIV, and two for the PLIF, which were then 'stitched' together to capture a wider region of interest (approximately 120×60 mm^2). The PIV images were processed with the open source MATLAB package PIVsuite (Vejražka, Zedníková & Stanovskỳ 2018), using a multi-pass interrogation with final window size 24×24 pixels. The PLIF images were processed using the algorithm developed by the present authors and discussed in detail in Milton-McGurk *et al.* (2020). This involves using images from the IDS uEye camera to obtain measurements of the laser power profile, and correcting each instantaneous PLIF image for variations in this power profile.

The flow is produced by injecting a mixture of freshwater, ethanol and Rhodamine 6G dye downwards into a 1 m^3 tank containing saltwater through a round pipe with diameter $D = 10$ mm. A schematic of this experimental set-up is given in figure 2. Rhodamine 6G is used as the fluorescence dye for the PLIF measurements, and the ethanol is added to the source mixture in order to match the refractive index with the saltwater ambient. By varying the ethanol and salt concentration of the source and ambient fluids, and adjusting the flow rate of the Ismatic MCP-Z gear pump used to drive the flow, source Froude and Reynolds numbers in the ranges $10 \lesssim Fr_o \lesssim 30$ and $2900 \lesssim Re_o \lesssim 6000$ were obtained. A list of the experiments performed in the present study, and those from Milton-McGurk *et al.* (2021), is given in table 1. The source and ambient fluid are prepared the day before a given experiment to ensure that the temperature is constant, and sufficient time is given between individual runs (approximately 30 min) to ensure that there is no motion in the tank. A schematic of a descending NBJ and fully developed fountain alongside processed PIV/PLIF images is shown in figure 3. Although only a small region of interest is observed in a given experiment (approximately 60×120 mm^2), data are gathered over a wider range of axial locations by repeating the experiment and adjusting the location of the inlet pipe and/or cameras.

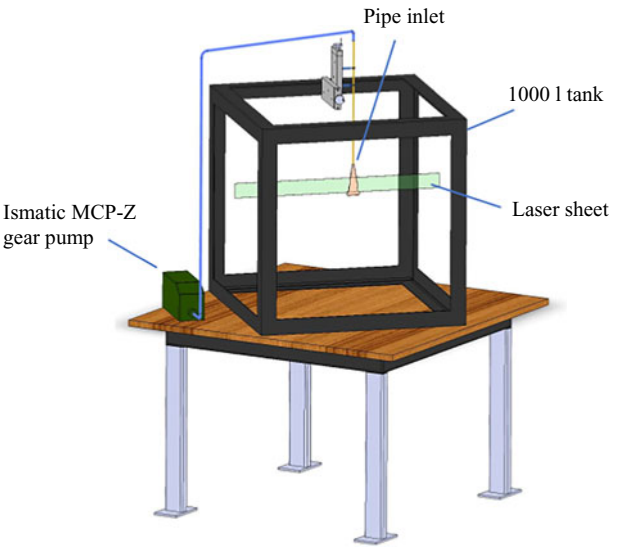

Figure 2. Illustration of the tank used in the present experimental set-up.

Flow	Fr_o	Re_o	z/D	w_o (mm s^{-1})	b_o (mm s^{-2})
F	30	6000	14–30	657	−95.9
F	20	6000	6–18	849	−354
F	15	4500	9–26	635	−358
F	10	3000	9–24	417	−347
NBJ	30	5800	18–39	635	−89.6
NBJ	20	6000	19–21	849	−354
NBJ	10	2900	9–12	417	−347
J	∞	5900	18–29	558	0

Table 1. Table summarising the experiments referred to in this study. All fountain experiments (F), and the $Fr_o = 10$ and 20 NBJs, were carried out for this investigation. The $Fr_o = 30$ NBJ and the neutral jet (J), were carried out in Milton-McGurk *et al.* (2021). All experiments had $D = 10$ mm.

Each experiment was optimised to gather data from either the initial NBJ stage of the flow, or the fully developed fountain stage. For the NBJ experiments, there is a much shorter time frame where it is possible to obtain data, so in a single 'run', images are captured at the maximum frequency of the system (7 Hz) and over a shorter overall time (e.g. 15 s), after which the flow is stopped. This would be repeated several times (e.g. 10 'runs') in order to obtain a sufficient number of images of the flow. Since a fully developed fountain is quasi-steady, these may be imaged for much longer time periods that are limited primarily by the memory and data transfer speed of the cameras. These runs were typically imaged at a lower frequency (e.g. 3 Hz) and for a longer time period (e.g. 100 s), allowing for more images to be captured overall per run. In principle, we are also limited by the tank volume since we are adding fluid during the experiment, but the time required to overflow the tank was always longer than the experiment time so this was not a decisive factor. The experimental set-up and image processing procedures were first benchmarked for a turbulent neutral jet, with additional details given in Milton-McGurk *et al.* (2020, 2021). In the following sections we will present data for fountains with $10 \leqslant Fr_o \leqslant 30$,

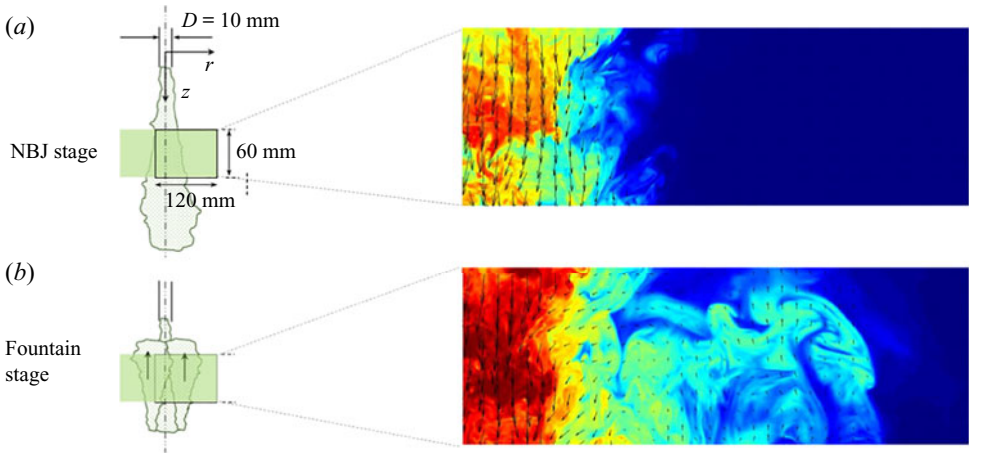

Figure 3. A schematic representation of (*a*) a descending NBJ and (*b*) a fully developed fountain, alongside processed PIV/PLIF images showing the scalar concentration field with overlaid velocity vectors. The approximate region of interest is indicated by the 120×60 mm^2 rectangle.

NBJs with $10 \leqslant Fr_o \leqslant 30$, and a neutral jet. Data for the $Fr_o = 30$ NBJ and neutral jet were obtained from the previous study, Milton-McGurk *et al.* (2021), while the remaining NBJ and fountain data are from the present investigation.

3. Flow statistics in fountains and NBJs

We will describe our flow locally using the local Froude and Richardson numbers, Fr and Ri,

$$Fr = \frac{w_m}{(-r_m b_m)^{1/2}} = \frac{1}{(-Ri)^{1/2}}, \tag{3.1}$$

where w_m, r_m and b_m are local velocity, length and buoyancy scales. These scales are defined in terms of the fluxes of volume, momentum and buoyancy, and the integral buoyancy, Q, M, F and B,

$$Q = 2\int_0^{\tilde{r}} \bar{w} r \,\mathrm{d}r, \quad M = 2\int_0^{\tilde{r}} \bar{w}^2 r \,\mathrm{d}r, \quad F = 2\int_0^{\tilde{r}} \bar{w}\bar{b} r \,\mathrm{d}r, \quad B = 2\int_0^{\tilde{r}} \bar{b} r \,\mathrm{d}r, \tag{3.2a–d}$$

which have been scaled to remove a factor π. Here, $w = w(r, z)$, $u = u(r, z)$ and $b = b(r, z)$ are the instantaneous axial and radial velocities, and buoyancy, which may be decomposed into their mean and fluctuating components, such as $w = \bar{w} + w'$. The buoyancy is defined as $b(r, z) = g(\rho(r, z) - \rho_a)/\rho_a$, where ρ is the local density, and r and z are the radial and axial coordinates. The time and azimuthal components have been omitted above for simplicity, since they are eliminated during the averaging process and under the assumption of statistical axis symmetry. This averaging is computed from multiple images in a given experiment, and across multiple repeated runs. Although NBJs do not strictly reach a steady state, it was shown in Milton-McGurk *et al.* (2020, 2021), that the flow is reasonably steady before the return flow forms, and that the mean profiles do not change considerably in this initial period. For an NBJ, the integration limit is $\tilde{r} = \infty$, resulting in the same definition that is commonly used for neutral/positively buoyant jets and plumes (Morton, Taylor & Turner 1956; Kaminski, Tait & Carazzo 2005; van Reeuwijk & Craske 2015). For a fully developed fountain, we set $\tilde{r} = r_{io}$, where r_{io} is the

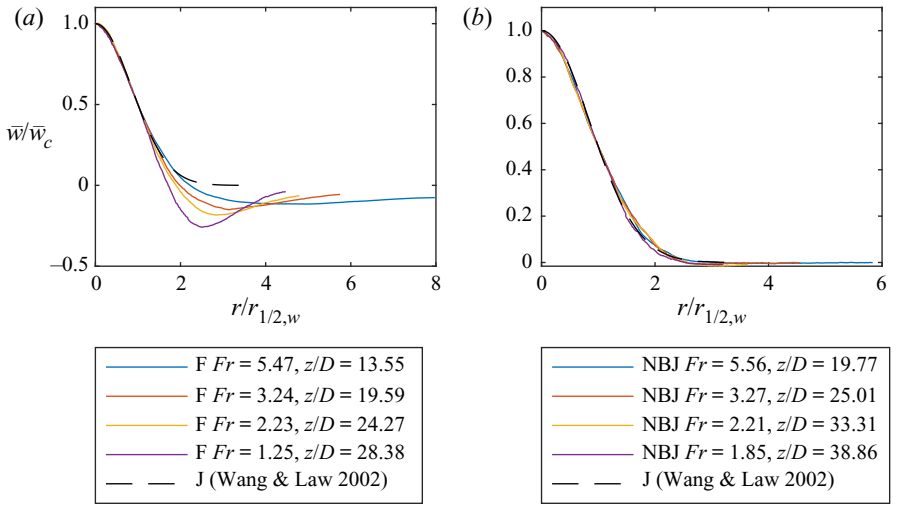

Figure 4. Mean velocity profiles, $\bar{w}$, for a fully developed fountain, (*a*), and NBJ (Milton-McGurk *et al.* 2021), (*b*), both with $Fr_o = 30$, at a range of axial locations. The profiles are normalised by the local centreline value, $\bar{w}_c$, and half-width, $r_{1/2,w}$. The best-fit profile for a neutral jet (J) by Wang & Law (2002) is also shown as a reference.

boundary between the IF and OF such that $\bar{w}(r = r_{io}) = 0$. These quantities allow us to define the local velocity, radius and buoyancy scales

$$w_m = \frac{M}{Q}, \quad r_m = \frac{Q}{M^{1/2}}, \quad b_m = \frac{BM}{Q^2}. \tag{3.3a–c}$$

3.1. *Velocity and buoyancy profiles*

Figures 4 and 5 show mean velocity and scalar concentration (buoyancy) profiles for fountains and NBJs with $Fr_o = 30$, along with the best-fit profile for a neutral jet by Wang & Law (2002) as a reference. Dimensionless scalar concentration ($0 \leqslant c \leqslant 1$) and buoyancy (mm s^{-2}) are related by a constant such that $b = c(\rho_o - \rho_a)g/\rho_a$. In Milton-McGurk *et al.* (2021), these profiles were shown to be Gaussian over a range of axial locations ($20 \lesssim z/D \lesssim 40$), or equivalently, local Froude numbers, Fr ($1.9 \lesssim Fr \lesssim 5.9$), in the NBJ, which are given in figures 4(*b*) and 5(*b*). When normalised by the centreline quantities, $\bar{w}_c$ and $\bar{c}_c$, and respective half-widths, $r_{1/2,w}$ and $r_{1/2,c}$, these velocity and scalar profiles in the NBJ collapse onto a single curve.

The profiles for a fully developed fountain obtained from the present experiments, also with $Fr_o = 30$, are shown in figures 4(*a*) and 5(*a*), where it is clear immediately that the profiles do not collapse in the same way as the NBJ. Although the velocity and scalar profiles are reasonably similar for $r/r_{1/2,w} \lesssim 1$ and $r/r_{1/2,c} \lesssim 1$, respectively, they diverge for radial locations beyond this. For the velocity profile, this is particularly evident in the OF where $\bar{w} < 0$. The minimum (most negative) value of the velocity profile will be denoted $\bar{w}_d$, with the radial location of this point denoted r_d. Figure 4(*a*) shows that $\bar{w}_d/\bar{w}_c$ becomes increasingly negative with increasing axial distance, while the location of the local minima, $r_d/r_{1/2,w}$, moves towards the centre. This is primarily a consequence of the normalisation, where $\bar{w}_c$ decreases strongly as the IF is decelerated under negative buoyancy, increasing the magnitude of $\bar{w}_d/\bar{w}_c$. The velocity half-width, $r_{1/2,w}$, also increases relative to r_d, reducing the value of $r_d/r_{1/2,w}$. The actual (non-normalised)

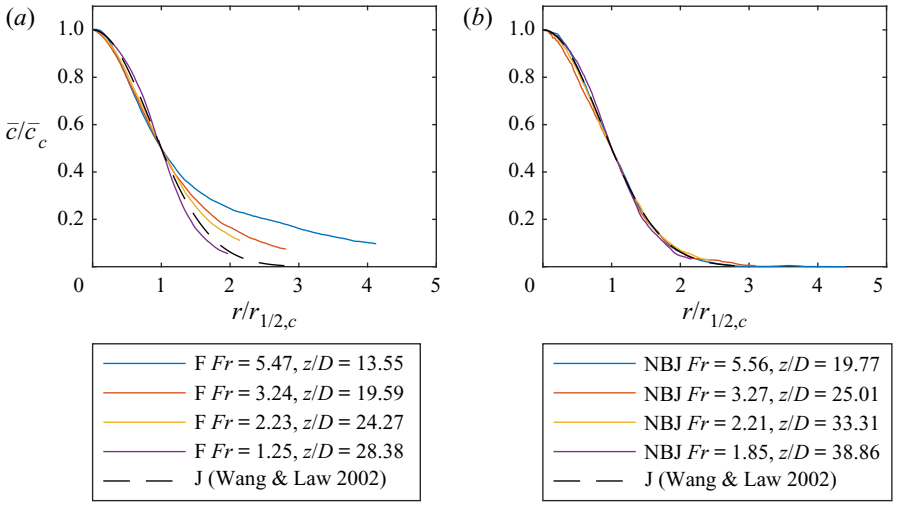

Figure 5. Mean scalar profiles, $\bar{c}$, for a fully developed fountain, (*a*), and NBJ (Milton-McGurk *et al.* 2021), (*b*), both with $Fr_o = 30$, at a range of axial locations. The profiles are normalised by the local centreline value, $\bar{c}_c$, and half-width, $r_{1/2,c}$. The best-fit profile for a neutral jet by Wang & Law (2002) is also shown as a reference.

magnitude of $\bar{w}_d$, however, decreases towards zero at the top of the fountain, and r_d moves outwards as the IF expands.

The scalar profiles, normalised by local quantities, are given in figures 5(*a*) and 5(*b*) for the fountain and NBJ. Unlike the NBJ profiles in figure 5(*b*), the fountain velocity profiles in figure 5(*a*) do not collapse onto the same curve for the full radial width, although they are reasonably similar in the inner profile for $r/r_{1/2,c} \lesssim 1$. This means that, particularly in the outer profile ($r/r_{1/2,c} \gtrsim 1$), they are no longer well described by a similar Gaussian shape along the flow, appearing to get narrower with axial distance. Neither the velocity or scalar (buoyancy) profiles in a fully developed fountain can therefore be considered self-similar in the sense that they have similar shapes along the fountain. Despite this, the most significant shape change of the profiles occurs in the return flow, with the inner profiles collapsing approximately when normalised by their centreline values and respective half-widths.

3.2. *Turbulence statistics*

Profiles for the axial turbulence fluctuations and Reynolds stress, $\overline{w'^2}$ and $\overline{w'u'}$, are given in figures 6 and 7, normalised by both local and source quantities. The development of these turbulence profiles in an NBJ was discussed in Milton-McGurk *et al.* (2021), where they were found to increase with axial distance due to the strongly decelerating mean flow, characterised here by $\bar{w}_c$. This differs from neutral jets and plumes, where $\overline{w'^2}$ and $\overline{w'u'}$ decrease at the same rate as the mean flow, so the normalised profiles, $\overline{w'^2}/\bar{w}_c^2$ and $\overline{w'u'}/\bar{w}_c^2$, are approximately constant along the flow (at least in the fully developed self-similar region) (Panchapakesan & Lumley 1993; Hussein, Capp & George 1994; Wang & Law 2002).

For the fully developed fountain, the behaviour of $\overline{w'^2}$ and $\overline{w'u'}$ remaining high relative to $\bar{w}_c^2$ is more prominent than in the NBJ. The normalised profiles in figures 6 and 7

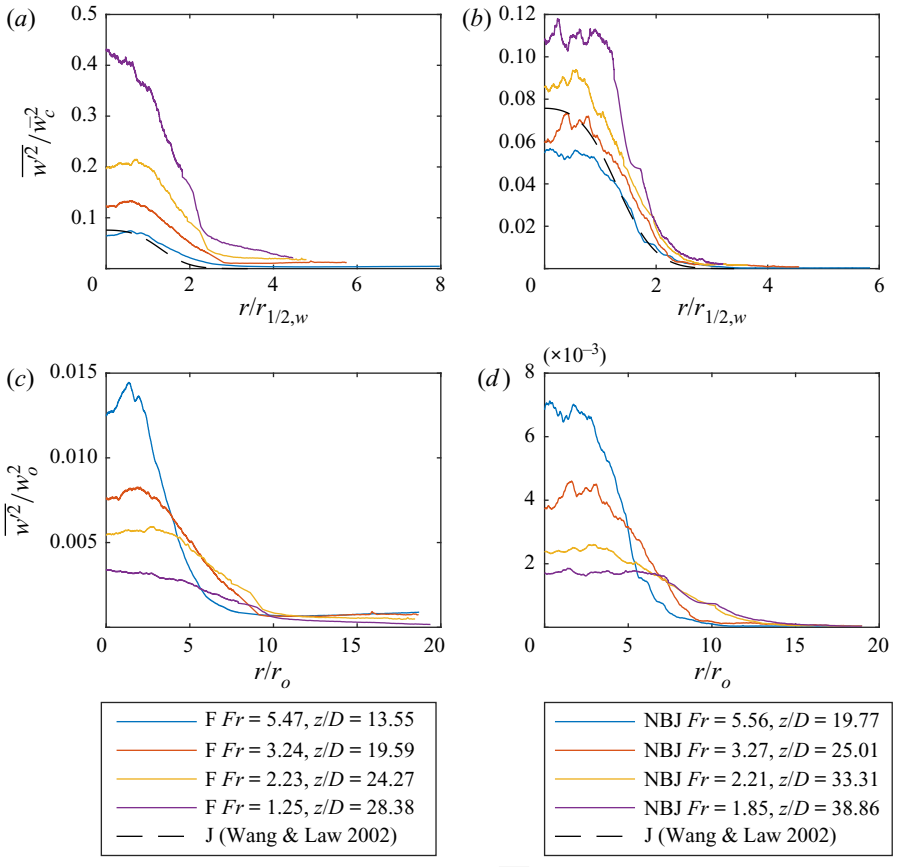

Figure 6. Profiles of the mean axial turbulence fluctuations, $\overline{w'^2}$, for a fully developed fountain, (*a*,*c*), and NBJ (Milton-McGurk *et al.* 2021), (*b*,*d*), both with $Fr_o = 30$. The profiles are normalised by the local centreline value, $\bar{w}_c^2$, and half-width, $r_{1/2,w}$, in (*a*,*b*), and by source velocity, w_o^2, and radius, r_o, in (*c*,*d*). The best-fit profile for a neutral jet by Wang & Law (2002) is also shown as a reference.

increase more rapidly in the fountain than in the NBJ, with large peak values $\overline{w'^2}/\bar{w}_c^2 \simeq 0.2$ and $\overline{w'u'}/\bar{w}_c^2 \simeq 0.04$ for the $Fr = 2.23$ profile. These are considerably higher than the NBJ peaks at a similar $Fr = 2.21$ of $\overline{w'^2}/\bar{w}_c^2 \simeq 0.09$ and $\overline{w'u'}/\bar{w}_c^2 \simeq 0.02$. Figures 6(*c*), 6(*d*), 7(*c*) and 7(*d*), which show the $\overline{w'^2}$ and $\overline{w'u'}$ profiles instead normalised by source conditions, illustrate the fact that the turbulence intensities are driven primarily by the decreasing $\bar{w}_c$, rather than by an increase in turbulence production. From these it is clear that $\overline{w'^2}$ and $\overline{w'u'}$ decrease with axial distance for both the NBJ and the fountain, and are higher in the fountain than the NBJ at similar local Fr. This is particularly true of the $\overline{w'^2}/w_o^2$ profile, where the peak values in the fountain profiles are approximately twice that of the NBJ at similar Fr. This is likely due to interactions between the IF and OF that result in increased turbulence in the IF, and so also contributes to the greater $\overline{w'^2}/\bar{w}_c^2$ and $\overline{w'u'}/\bar{w}_c^2$ observed in the fountain. Cresswell & Szczepura (1993) also gathered turbulence data for a fully developed fountain, although one with a much lower $Fr_o \simeq 3.2$ ($z_{ss}/D \simeq 3.9$). When normalised by the local centreline value, their peak axial turbulence intensity was $\overline{w'^2}/\bar{w}_c^2 \simeq 0.046$ near the source at $z/D = 0.3$, which increased to $\overline{w'^2}/\bar{w}_c^2 \simeq 1.8$ near the

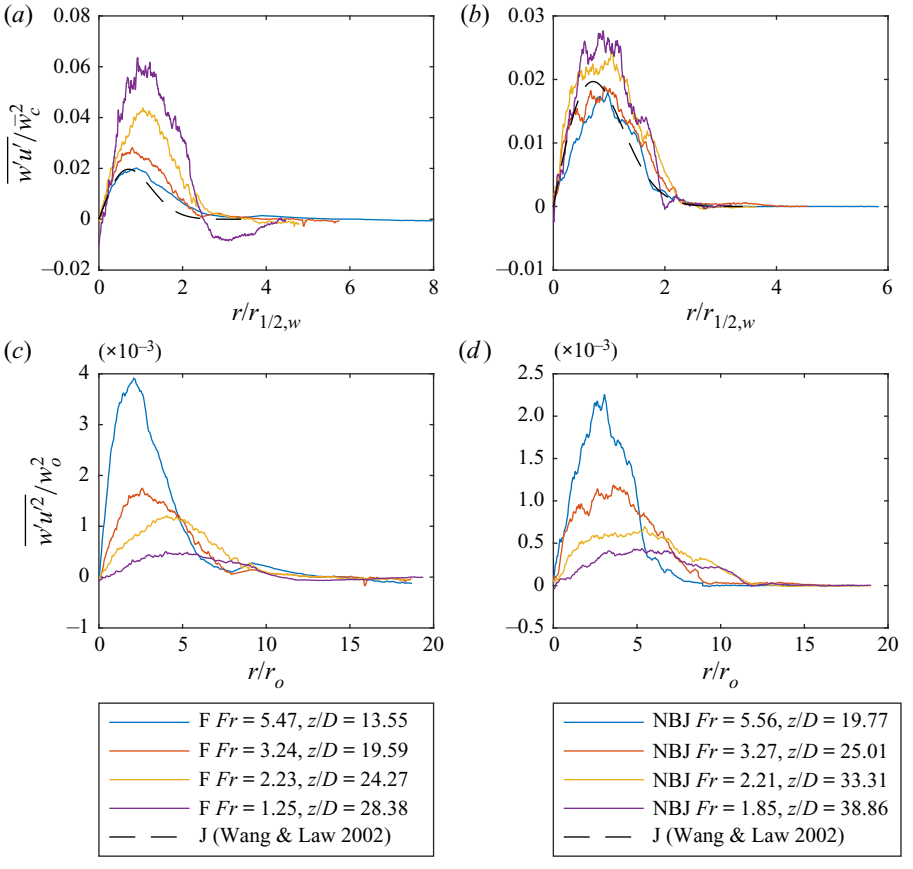

Figure 7. Profiles of the mean Reynolds stress, $\overline{w'u'}$, for a fully developed fountain, (*a*,*c*), and NBJ (Milton-McGurk *et al.* 2021), (*b*,*d*), both with $Fr_o = 30$. The profiles are normalised by the local centreline value, $\bar{w}_c^2$, and half-width, $r_{1/2,w}$, in (*a*,*b*), and by source velocity, w_o^2, and radius, r_o, in (*c*,*d*). The best-fit profile for a neutral jet by Wang & Law (2002) is also shown as a reference.

cap at $z/D = 3$. Although the magnitudes at a given axial location differ from the present data due to the significantly different Fr_o, the observation of $\overline{w'^2}/\bar{w}_c^2$ increasing as the flow decelerates is consistent with our higher Fr_o fountains.

Figures 8(*a*) and 8(*b*) show profiles of the mean turbulence scalar fluctuations, $\sqrt{\overline{c'^2}}/\bar{c}_c$, for the fountain and NBJ, respectively. The NBJ profiles are reasonably well collapsed, while the fountain profiles are not self-similar and also do not appear to follow a clear increasing or decreasing trend with axial distance. Profiles of the axial and radial fluxes, $\overline{w'c'}$ and $\overline{u'c'}$, for the fountain and NBJ are given in figures 9 and 10. When normalised by local quantities, these profiles clearly increase with axial distance. A moderate increase can also be observed between the NBJ profiles nearest and furthest from the source ($z/D =$ 19.77 and $z/D = 38.86$), although the trend is less significant and there is some scatter in the profiles between these locations. As with the velocity fluctuations, the growth in the turbulent scalar profiles for the fountain is primarily a result of normalising by the decreasing $\bar{w}_c$, rather than an increase in axial/radial scalar transport. It is also notable that the $\overline{w'c'}$ profiles for the fountain drop considerably below zero in the outer profile.

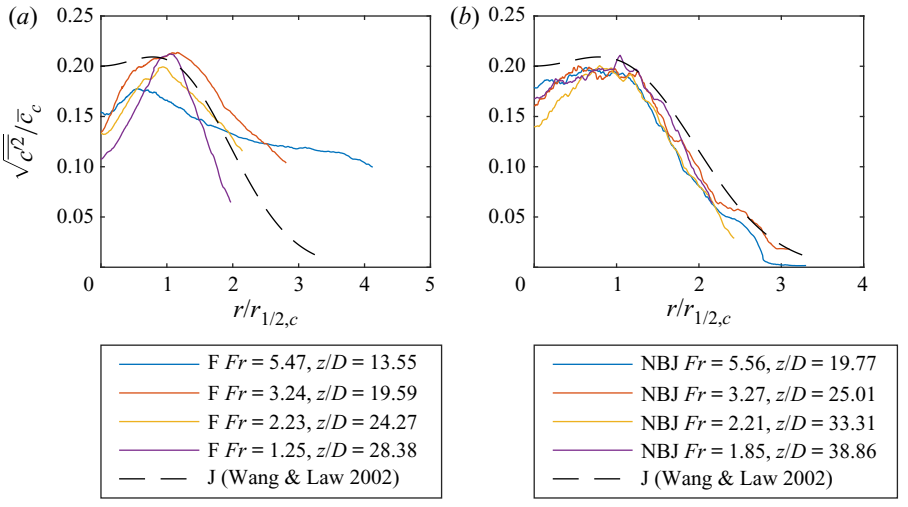

Figure 8. Profiles of the mean scalar fluctuations, $\sqrt{\overline{c'^2}}$, for a fully developed fountain, (*a*), and NBJ (Milton-McGurk *et al.* 2021), (*b*), both with $Fr_o = 30$. The profiles are normalised by the local centreline value, $\bar{c}_c$, and half-width, $r_{1/2,c}$. The best-fit profile for a neutral jet by Wang & Law (2002) is also shown as a reference.

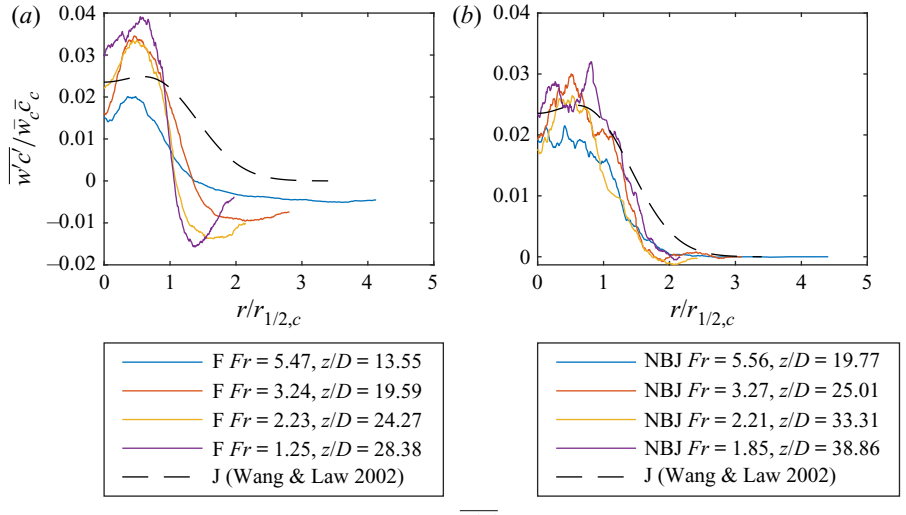

Figure 9. Profiles of the mean axial turbulent flux, $\overline{w'c'}$, for a fully developed fountain, (*a*), and NBJ (Milton-McGurk *et al.* 2021), (*b*), both with $Fr_o = 30$. The profiles are normalised by the local product, $\bar{w}_c\bar{c}_c$, and half-width, $r_{1/2,c}$. The best-fit profile for a neutral jet by Wang & Law (2002) is also shown as a reference.

This corresponds to the OF region where the direction of axial mean flow is reversed, and so a sign reversal of the axial scalar flux is expected.

Mean and turbulence statistics have been presented for a fully developed fountain and an NBJ, both with $Fr_o = 30$, at axial locations where they have a similar local Fr. Presenting these fountain profiles alongside those for an NBJ with the same Fr_o allows the effect of a return flow to be revealed. In the fountain, although the $\bar{w}/\bar{w}_c$ and $\bar{c}/\bar{c}_c$ profiles collapse approximately in the IF, they do not maintain similar shapes in the OF and are therefore not generally self-similar. This is in contrast to the NBJ, which does not have

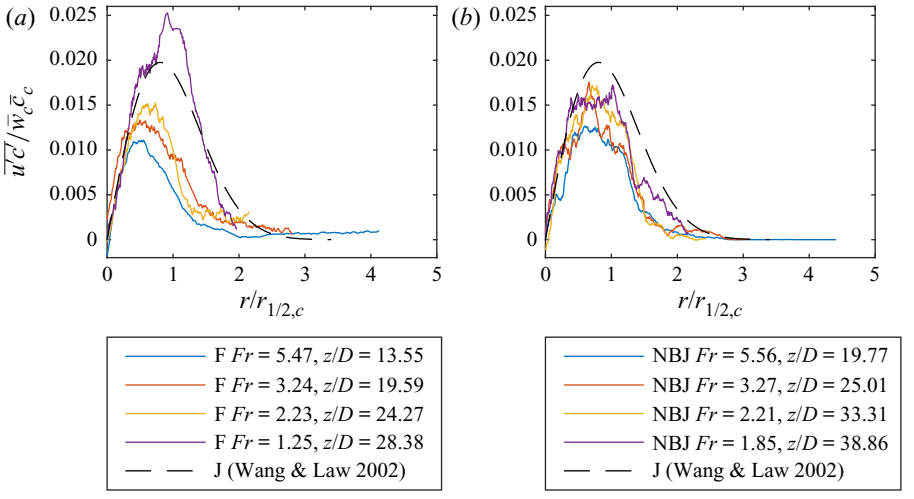

Figure 10. Profiles of the mean radial turbulent flux, $\overline{u'c'}$, for a fully developed fountain, (*a*), and NBJ (Milton-McGurk *et al.* 2021), (*b*), both with $Fr_o = 30$. The profiles are normalised by the local product, $\bar{w}_c\bar{c}_c$, and half-width, $r_{1/2,c}$. The best-fit profile for a neutral jet by Wang & Law (2002) is also shown as a reference.

an OF, and has Gaussian velocity and scalar profiles over the full range of observed Fr locations. The presence of a return flow tends to increase turbulence in the IF of fountains, which can be seen by the significantly larger $\overline{w'^2}/\bar{w}_c^2$ and $\overline{w'u'}/\bar{w}_c^2$ compared to an NBJ at similar Fr locations. In both fountains and NBJs, the turbulence profiles involving velocity fluctuations, namely $\overline{w'u'}$, $\overline{w'^2}$, $\overline{u'c'}$ and $\overline{w'c'}$, all increase with axial distance when normalised by centreline values. This is primarily a result of the strongly decelerating mean flow, characterised here by $\bar{w}_c$, rather than an increase in turbulence along the flow. This observation was first noted in Milton-McGurk *et al.* (2021) for NBJs, with the present study identifying a similar behaviour in fountains.

Figures 4–10 have all shown profiles normalised by the local mean centreline values. Another potential scaling option would be to include the OF velocity, which could be characterised by the velocity at the location of 'maximum outer flow', $\bar{w}(r = r_d) = \bar{w}_d$. The mean velocity profile could then be normalised by a characteristic relative IF/OF velocity, $\bar{w}_c - \bar{w}_d$. However, since $\bar{w}_c \gg |\bar{w}_d|$ for the majority of the fountain height, this gives results similar to those for the $\bar{w}_c$ normalisation, and the profiles do not collapse across the full fountain width. Another approach would be to consider the quantity $(\bar{w} - \bar{w}_d)/(\bar{w}_c - \bar{w}_d)$, which is the fountain velocity relative to the moving reference frame of the OF. This is always positive and has centreline value 1. Although this could potentially be useful from a modelling point of view, it also did not collapse the present results over the full fountain width.

4. Fr_o dependence

Statistics for two fountains with different source Froude numbers, $Fr_o = 30$ and 15, will now be presented at locations with similar local Fr. Figures 11(*a*) and 11(*b*) show the $\bar{w}/\bar{w}_c$ and $\bar{c}/\bar{c}_c$ profiles for both these fountains at $Fr = 3.1$ and $Fr = 1.3$. The velocity profiles in figure 11(*a*) with matching local Fr are very similar for $0 \lesssim r \lesssim r_d$ at both Fr locations – that is, up to approximately the radial location of 'maximum return flow'. The profiles with $Fr = 3.1$ are similar even beyond this point, over the full r range obtained, although

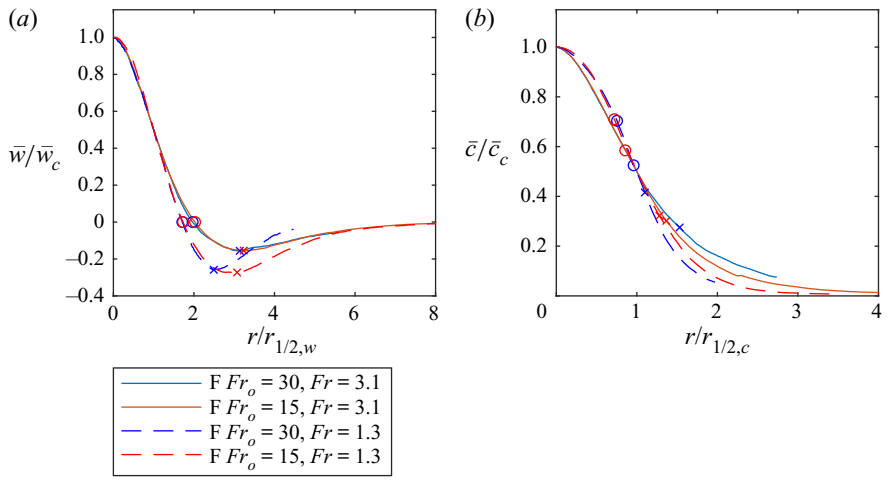

Figure 11. Normalised (*a*) $\bar{w}$, and (*b*) $\bar{c}$, profiles in $Fr_o = 30$ and 15 fountains. The profiles correspond to axial locations where the local Fr in both flows are approximately equal. Additionally, ○ markers corresponding to radial location, r_{io}, and × markers corresponding to r_d, are shown on each profile.

this is not the case at all Fr locations. The scalar profiles in figure 11(*b*) are also similar in this r range, where they agree up to near the × markers that correspond to r_d, while differing somewhat in the outer profile.

The agreement of these profiles between the two Fr_o fountains at similar Fr is better than for those in figures 4(*a*) and 5(*a*), which showed profiles at different Fr locations for the same $Fr_o = 30$ fountain. The latter $\bar{w}/\bar{w}_c$ profiles agreed only up until $r/r_{1/2,w} \lesssim 1$, which is prior to the IF/OF boundary, r_{io}. The $\bar{c}/\bar{c}_c$ profiles in figure 5(*a*) agree only approximately for $r/r_{1/2,w} \lesssim 1$, and are significantly different beyond this. In figure 11(*b*), the agreement between the $Fr_o = 30$ and 15 profiles is closer over the full profiles shown, but particularly for $r/r_{1/2,c} \lesssim 1$. Together, figures 4, 5 and 11 show that despite the locally normalised velocity/scalar profiles not being generally self-similar within an individual fountain, their shape for $r \lesssim r_d$ does not depend significantly on Fr_o and instead appears to be scaled with Fr. That is, at a given local Fr, these profiles in different Fr_o fountains are similar up to the location of maximum return flow, r_d, with the closest agreement up to the IF/OF boundary, r_{io}. For $r \lesssim r_d$, the mean profiles in fountains are therefore well characterised by Fr, which depends only on IF quantities. This implies that the local IF width of a fountain scales with Fr, which is comparable to previous studies that suggest that the overall width of a fountain scales with Fr_o (Mizushina *et al.* 1982). It should be noted that both fountains in figure 11 have Fr_o in the 'highly forced' regime ($Fr_o \gtrsim 5.5$), and this may not hold in lower Fr_o fountains, particularly those in the 'intermediate' regime and below ($Fr_o \lesssim 2.8$) (Burridge & Hunt 2012).

Figure 12 shows $\overline{w'u'}/\bar{w}_c^2$ and $\overline{u'c'}/\bar{w}_c\,\bar{c}_c$ for both $Fr_o = 30$ and 15 fountains at similar Fr locations. In contrast to the mean velocity/scalar profiles in figure 11, these turbulence quantities clearly have both an Fr and an Fr_o dependence, and are not generally similar in the two fountains at the same Fr. This difference is likely due to interactions with the OF having an effect on the turbulence production in the IF, since the OF at a given Fr location will be different in $Fr_o = 30$ and 15 fountains. Although differences in the OF may also affect the mean profiles, $\bar{w}$ and $\bar{c}$ in the IF, this is largely captured by $\bar{w}_c$ and $\bar{c}_c$ in the normalisation. An Fr_o dependence in $\overline{w'u'}/\bar{w}_c^2$ and $\overline{u'c'}/\bar{w}_c\,\bar{c}_c$ at similar Fr locations is not

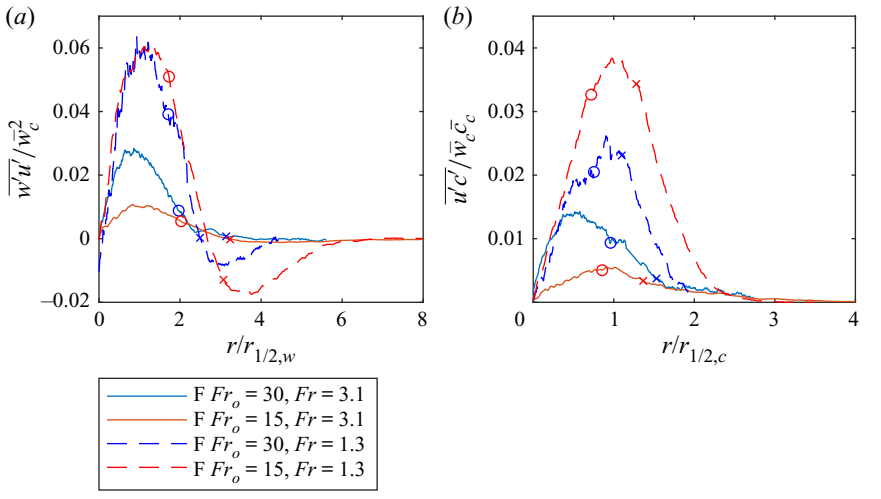

Figure 12. Normalised (*a*) $\overline{w'u'}$, and (*b*) $\overline{u'c'}$, profiles in $Fr_o = 30$ and 15 fountains. The profiles correspond to axial locations where the local Fr values in both flows are approximately equal. Additionally, ○ markers corresponding to radial location, r_{io}, and × markers corresponding to r_d, are shown on each profile.

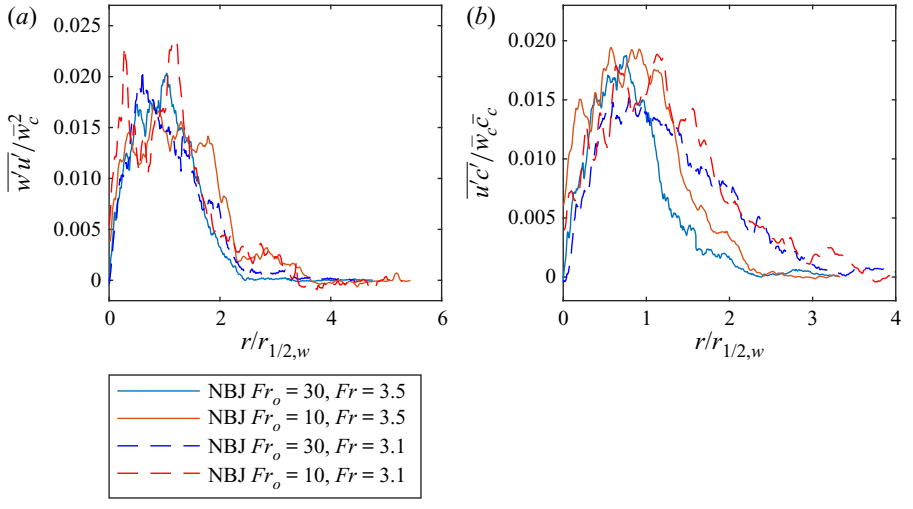

Figure 13. Normalised (*a*) $\overline{w'u'}$, and (*b*) $\overline{u'c'}$, profiles in $Fr_o = 30$ (Milton-McGurk *et al.* 2021) and $Fr_o = 10$ (present study) NBJs. The profiles correspond to axial locations where the local Fr values in both flows are approximately equal.

seen in NBJs, which do not have an OF present. This can be seen in figure 13, which show the profiles for NBJs with $Fr_o = 30$ (Milton-McGurk *et al.* 2021) and $Fr_o = 10$ (present study) at locations corresponding to $Fr \simeq 3.5$ and $Fr \simeq 3.1$. Although these are somewhat noisier than in the fountain, both the $\overline{w'u'}/\bar{w}_c^2$ and $\overline{u'c'}/\bar{w}_c\,\bar{c}_c$ profiles have similar shapes and magnitudes at the two Fr locations. This supports the hypothesis that the Fr_o dependence observed in figure 12 for the fountain is primarily a result of the return flow, which is not present in the NBJ.

5. Centreline velocity decay

Figure 14(*a*) shows the decay of the centreline velocity, characterised by $w_o/\bar{w}_c$, for $10 \leqslant Fr_o \leqslant 30$ fountains and NBJs plotted with z/D. Data for a neutral jet, which has $Fr = \infty$,

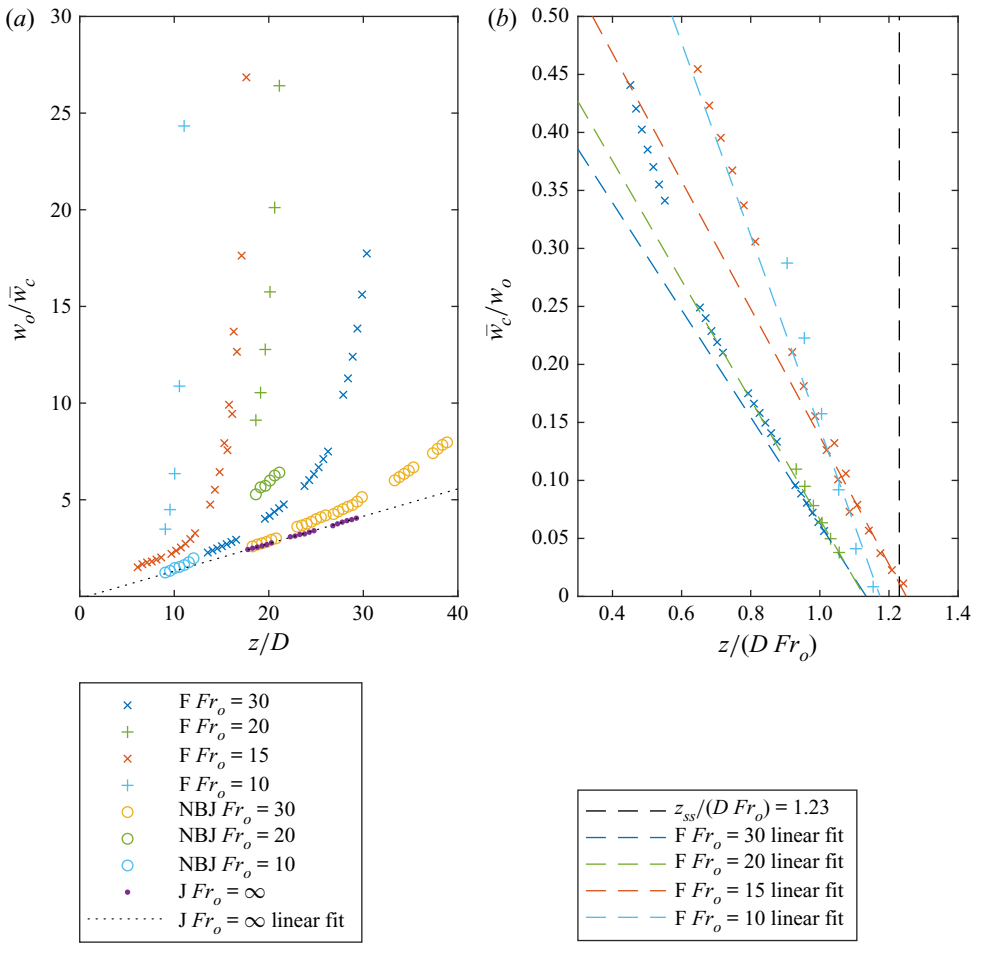

Figure 14. The decay of the mean centreline velocity, $w_o/\bar{w}_c$, plotted with z/D in (*a*), and $\bar{w}_c/w_o$ plotted with $z/(DFr_o)$ in (*b*), for fountains and NBJs with $10 \leqslant Fr_o \leqslant 30$, and a neutral jet. In (*b*), a vertical line corresponding to the steady-state height of a fountain as predicted by $z_{ss}/r_o = 2.46\,Fr_o$ is also shown (Turner 1966; Burridge & Hunt 2012). Data for the $Fr_o = 30$ NBJ and the neutral jet were obtained from Milton-McGurk *et al.* (2021), while the remaining NBJ and fountain data are from the present study.

are also shown as a reference. The neutral jet and $Fr_o = 30$ NBJ data were obtained from Milton-McGurk *et al.* (2021), while the remaining NBJ and fountain data are from the present study. In neutral jets, the velocity decay corresponds to a $\bar{w}_c^{-1} \sim z$ scaling. In NBJs, this deceleration is stronger and the relationship between $\bar{w}_c^{-1}$ and z is generally nonlinear. Near the source, however, where the local Fr is high and the flow is momentum dominated, NBJs are more similar to neutral jets and $w_o/\bar{w}_c$ could be approximated as linear. This region was referred to as the 'forced' regime in Milton-McGurk *et al.* (2021), and corresponds approximately to $z/D \lesssim 26$ ($Fr \gtrsim 3.0$) for the $Fr_o = 30$ NBJ.

At similar z/D locations, the $Fr_o = 10$, 20 and 30 fountains all decelerate more rapidly than the corresponding NBJ with the same Fr_o. This is most evident in the $Fr_o = 30$ case, where data have been gathered over a larger z/D range, and reveal the significance of the return flow on the development of $\bar{w}_c$. The $Fr_o = 10$ NBJ data, which are close to the source and in the 'forced' regime, almost coincide with the linear fit of the jet data. It is

possible that all NBJs with sufficiently high Fr_o approach this 'neutral jet line' near the source where the flow is increasingly momentum-dominated, although additional research is required to affirm this. For fountains, $w_o/\bar{w}_c$ may never closely resemble this jet-like state, since the presence of the return flow will continue to affect the IF even at the source.

In figure 14(*b*), $\bar{w}_c/w_o$ for the fountains is plotted with $z/(D\,Fr_o)$, along with a vertical line at the location $z/(D\,Fr_o) = 1.23$. This corresponds to the steady-state rise height predicted by the scaling relation $z_{ss}/r_o = 2.46\,Fr_o$ (Turner 1966; Kaye & Hunt 2006; Burridge & Hunt 2012), which has been shown to hold for forced fountains with $Fr_o \gtrsim 3$. The location where $\bar{w}_c/w_o = 0$ corresponds to z_{ss}, and since data were not gathered at the top of the cap region where where the velocity is fully reduced to zero and z_{ss} is reached, linear fits of $\bar{w}_c/w_o$ for the present data have also been shown so that the data may be extrapolated to this point. Because $\bar{w}_c/w_o$ is not linear over the entire fountain height, these fits were based on data near the top, $z/(DFr_o) \gtrsim 1$, where a linear trend may be a reasonable approximation over short distances. This slightly under-predicts $z_{ss}/(D\,Fr_o) = 1.23$ for the $Fr_o = 30$, 20 and 10 fountains, and slightly over-predicts it for $Fr_o = 15$, but in all cases is within approximately 1–8 % of the scaling relation.

6. Radial expansion and fountain width

The radial expansion of the IF of the fountains may may be characterised by the radial location of the IF/OF boundary, r_{io}, or by other measures of the IF velocity profile, such as the half-width, $r_{1/2,w}$. Figure 15(*a*) shows $r_{1/2,w}/D$ with axial distance, z/D, for the fountains, the NBJs and a neutral jet (Milton-McGurk *et al.* 2021). For the $Fr_o = 30$ and 15 fountains, r_{io}/D is also shown. For a large portion of their height, the neutral jet, fountains and NBJs all have similar $r_{1/2,w}/D$ at similar axial locations, and follow an approximately linear trend. Mizushina *et al.* (1982) had a similar finding in their experimental study on fully developed fountains, where they found that a linear correlation, $r_{io} = 0.17z$, described approximately the location of the IF/OF boundary for a wide range of Fr_o fountains ($3 \lesssim Fr_o \lesssim 258$). This relation is shown in figure 15(*a*), alongside a linear fit based on the present $Fr_o = 15$ and 30 data of $r_{io}/D = 0.16z$, which is in reasonable agreement. The $Fr_o = 10$ and 20 fountains were not included in this correlation, since, as will be discussed in the next paragraph, data for these flows were obtained only in the cap region. It should be emphasised that any linear relations of r_{io} or $_{1/2,w}$, in either fountains or NBJs, are only approximations, and become less valid towards the cap region where $Fr \to 0$.

In the $Fr_o = 15$ and 30 fountains, $r_{1/2,w}$ and r_{io} increase with z/D for the majority of their height, followed by a sharp decrease after some critical point. Since the overall width of a fountain decreases in the cap region, the internal IF width scales could also be expected to decrease in the cap. The location where r_{io} and $r_{1/2,w}$ start to decline may therefore reflect the beginning of the cap region, which will be denoted z_c. For the $Fr_o = 10$ and 20 fountains, all data shown are within the cap region ($z \gtrsim z_c$), which is reflected by the decreasing $r_{1/2,w}$. For the $Fr_o = 15$ and 30 fountains, the IF width begins decreasing at $z_c/D \simeq 15$ and $z_c/D \simeq 28$, respectively. The same values are obtained using either the location of maximum $r_{1/2,w}$ or r_{io}, and are approximately $z_c/D \simeq Fr_o$ for both fountains. Vertical lines are also shown in figure 15(*a*) to indicate the predicted steady-state rise height of these fountains based on the high Fr_o scaling relation, $z_{ss}/r_o = 2.46\,Fr_o$ (Turner 1966; Kaye & Hunt 2006; Burridge & Hunt 2012). If the cap region were assumed hemispherical, then the thickness of the cap would be an approximation of the overall fountain radius, r_f. If, additionally, $z_c/D = Fr_o$ was presumed to be a universal scaling for

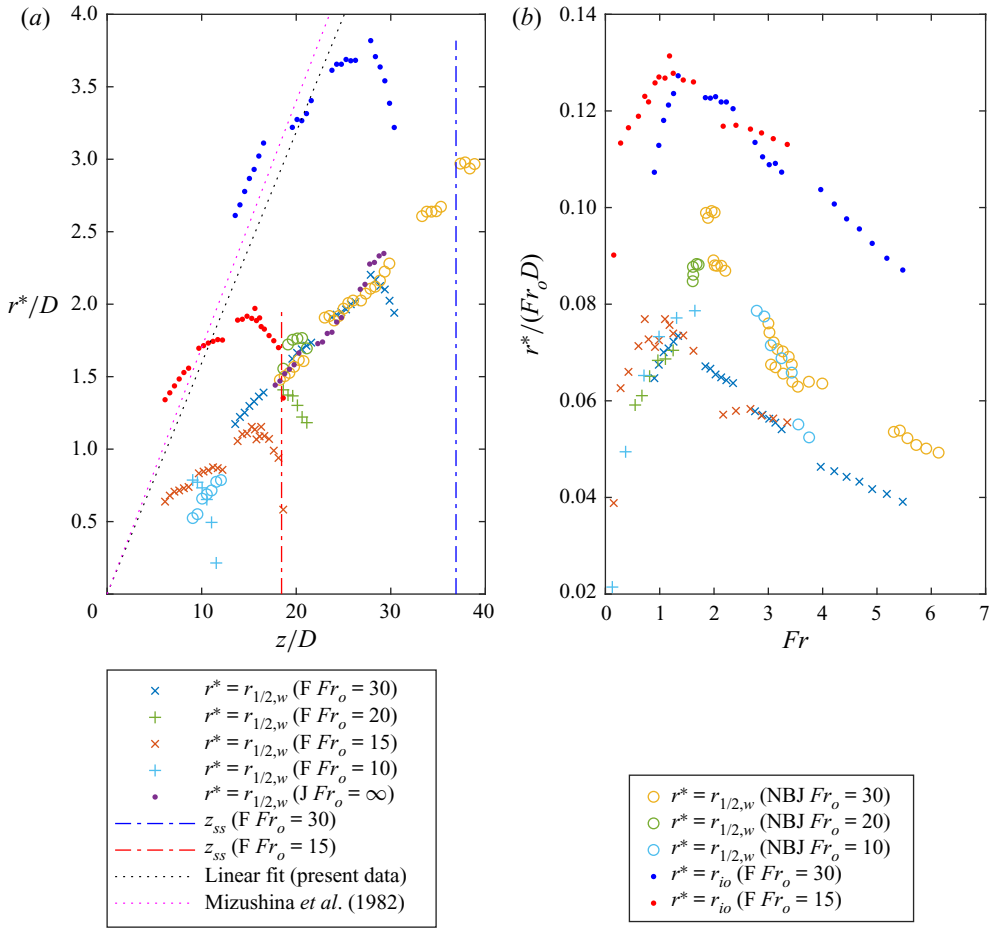

Figure 15. The velocity half-width, $r_{1/2,w}$, for $10 \leqslant Fr_o \leqslant 30$ fountains and NBJs, and a neutral jet. The radial location of the IF/OF boundary, r_{io}, is also shown for the $Fr_o = 15$ and 30 fountains. In (*a*), $r_{1/2,w}/D$ and r_{io}/D are plotted against z/D, with vertical lines showing the locations of the steady-state rise height, z_{ss}/D, of the $Fr_o = 15$ and 30 fountains. In (*b*), an alternative normalisation is used, $r_{1/2,w}/(Fr_o\, D)$ and $r_{io}/(Fr_o\, D)$, plotted with Fr.

the start of the cap region, then by using the aforementioned z_{ss} relation, we obtain

$$\frac{r_f}{D} = \frac{z_{ss}}{D} - \frac{z_c}{D} = 0.23\, Fr_o. \tag{6.1}$$

This is in good agreement with the proposed relation $r_f/D = 0.26\, Fr_o$ by Mizushina *et al.* (1982), who measured the width of fountains directly with $3 \lesssim Fr_o \lesssim 258$. The agreement supports the earlier assumption that the location of maximum r_{io} and $r_{1/2,w}$ can be used to estimate the start of the cap region.

Figure 15(*b*) shows the radial expansion of the IF normalised by Fr_o, with $r_{1/2,w}/(Fr_o\, D)$ and $r_{io}/(Fr_o\, D)$ plotted against Fr. The start of the cap region occurs at similar Fr for the $Fr_o = 15$ and 30 fountains, at $Fr = 1.1$ and 1.3, respectively. These are similar to the value $Fr = 1.4$ proposed by Shrinivas & Hunt (2014) and used by Hunt & Debugne (2016) in their theoretical model of a fountain. Although there is some scatter in the data in figure 15(*b*), the values of $r_{1/2,w}/(Fr_oD)$ are in reasonable agreement at similar Fr for all Fr_o fountains shown.

This is consistent with the arguments made in § 4 with regard to figure 11(*a*), where the shapes of the velocity profiles in the IF are not affected significantly by Fr_o, and are instead governed by Fr. Figure 15(*b*) is then an alternative way of showing that the IF width scales with the local Fr, just as the overall fountain width scales with the source Froude number, Fr_o, as was reported by Mizushina *et al.* (1982) and implied by (6.1).

7. Integral models

7.1. *Jet and plume models*

Morton *et al.* (1956) proposed an integral model, referred to here as the MTT model, based on the conservation of mass, momentum and buoyancy, to describe plumes originating from a point source. These may also be applied to neutral and buoyant jets, as well as NBJs prior to the return flow forming (Morton 1959; Milton-McGurk *et al.* 2021). The MTT model invokes the 'entrainment assumption', which relates the radial inflow of ambient fluid into the jet to a characteristic vertical velocity at that height by an 'entrainment coefficient', α. Simple applications of the model, such as to pure plumes (zero initial momentum) and neutral jets (zero buoyancy), typically use a constant value of α in the range $0.10 \lesssim \alpha_p \lesssim 0.16$ and $0.065 \lesssim \alpha_j \lesssim 0.080$ for plumes and jets, respectively (Fischer *et al.* 1979; Carazzo, Kaminski & Tait 2006). Priestley & Ball (1955) also developed an integral model for plumes/jets, referred to here as the PB model, but instead derived from the conservation of momentum, buoyancy and kinetic energy. Although the PB model did not make use of the entrainment assumption originally, Fox (1970) showed how when combined with the continuity equation, it implies that α is a function of the local Ri. For flows with constant Ri, such as pure jets and plumes, α is then constant and the MTT model is obtained (Fox 1970; Fischer *et al.* 1979). Analytical solutions to these models can be obtained by assuming fully self-similar velocity and buoyancy profiles in the flow, where the shapes of the profiles are assumed to be Gaussian or 'top-hat' (constant inside the plume/jet, zero outside it). More recent studies have developed these models further, by omitting assumptions about the shapes or self-similarity of the profiles (Kaminski *et al.* 2005; van Reeuwijk & Craske 2015).

These more recent formulations of the models may be derived from the conservation of volume, momentum, buoyancy and kinetic energy equations for a high-Re_o axisymmetric flow in a homogeneous environment (Kaminski *et al.* 2005; van Reeuwijk & Craske 2015):

$$\frac{\partial}{\partial r}(r\bar{u}) + \frac{\partial}{\partial z}(r\bar{w}) = 0, \tag{7.1}$$

$$\frac{\partial}{\partial r}(r\bar{u}\,\bar{w} + r\overline{u'w'}) + \frac{\partial}{\partial z}(r\bar{w}^2) = r\bar{b}, \tag{7.2}$$

$$\frac{\partial}{\partial r}(r\bar{u}\bar{b} + r\overline{u'b'}) + \frac{\partial}{\partial z}(r\bar{w}\bar{b}) = 0, \tag{7.3}$$

$$\frac{\partial}{\partial r}(r\bar{u}\,\bar{w}^2 + 2r\overline{u'w'}\bar{w}) + \frac{\partial}{\partial z}(r\bar{w}^3) = 2r\overline{u'w'}\,\frac{\partial \bar{w}}{\partial r} + 2r\bar{w}\bar{b}. \tag{7.4}$$

Pressure contributions and second-order turbulence terms, namely those involving $\overline{w'^2}$ and $\overline{w'b'}$, are neglected here. Neglecting these higher-order terms is common in the jet and plume literature, where they are typically found to be negligible (Wang & Law 2002; Kaminski *et al.* 2005; van Reeuwijk & Craske 2015; van Reeuwijk *et al.* 2016). For the case of fountains and NBJs, these terms have been estimated as they appear after integrating

(7.1)–(7.4), and are also found to be small compared to the mean components for the majority of the flow. The terms become larger near the top of an NBJ/fountain, where the mean velocity goes to zero and there is non-zero turbulence, but this region is not considered in the present analysis.

For neutral or positively/negatively buoyant jets in a quiescent homogeneous ambient, these equations may be integrated to infinity, with respect to r, to obtain a set of ordinary differential equations (ODEs) consistent with the MTT and PB models (Priestley & Ball 1955; Morton *et al.* 1956; Kaminski *et al.* 2005; van Reeuwijk & Craske 2015):

$$\frac{\mathrm{d}Q}{\mathrm{d}z} = 2\alpha M^{1/2}, \tag{7.5}$$

$$\frac{\mathrm{d}M}{\mathrm{d}z} = B = \frac{FQ}{\theta_m M}, \tag{7.6}$$

$$\frac{\mathrm{d}F}{\mathrm{d}z} = 0, \tag{7.7}$$

$$\frac{\mathrm{d}}{\mathrm{d}z}\left(\gamma_m \frac{M^2}{Q}\right) = \delta_m \frac{M^{5/2}}{Q^2} + 2F, \tag{7.8}$$

where the entrainment coefficient, α, is defined as

$$(r\bar{u})_{r=\tilde{r}} = -\alpha r_m w_m. \tag{7.9}$$

The quantities θ_m, γ_m and δ_m are 'profile coefficients' corresponding to the dimensionless buoyancy flux, mean kinetic energy and turbulence production, and are constant if the flow is fully self-similar:

$$\left.\begin{aligned} \theta_m &= \frac{F}{w_m b_m r_m^2}, \\ \gamma_m &= \frac{2}{w_m^3 r_m^2}\int_0^{\tilde{r}} \bar{w}^3 r\,\mathrm{d}r, \\ \delta_m &= \frac{4}{w_m^3 r_m}\int_0^{\tilde{r}} \overline{w'u'}\,\frac{\partial \bar{w}}{\partial r}\,r\,\mathrm{d}r. \end{aligned}\right\} \tag{7.10}$$

In the present context of neutral or positively/negatively buoyant jets and plumes, the integration limit is set to $\tilde{r} = \infty$ in all definitions.

For a constant α, (7.5)–(7.7) then represent the MTT model in the case of self-similar flow, with the value of θ_m depending on the assumed profile shapes (e.g. $\theta_m = 1$ for top-hat profiles). van Reeuwijk & Craske (2015) used (7.5)–(7.8) to derive an analytical expression for α that does not make any assumptions about the shape of the profiles or whether they are self-similar:

$$\alpha = -\frac{\delta_m}{2\gamma_m} + \left(1 - \frac{\theta_m}{\gamma_m}\right) Ri + \frac{Q}{2M^{1/2}}\frac{\mathrm{d}}{\mathrm{d}z}(\ln \gamma_m). \tag{7.11}$$

For a self-similar neutral jet, which has $Ri = 0$ and constant profile coefficients, the second two terms are zero and a constant entrainment coefficient is obtained, while for self-similar buoyant jets, α follows a linear relationship with Ri. In a previous study, the present authors calculated the terms of (7.11) for an $Fr_o = 30$ NBJ after assuming Gaussian velocity and buoyancy profiles (Milton-McGurk *et al.* 2021). It was found that α could be approximated reasonably by a constant $\theta_m \simeq 0.64$ and linear fit of δ_m with Ri, giving a linear relationship

between α and Ri. Since $Ri \to -\infty$ as $w_m \to 0$ at the top of an NBJ, α decreases with axial distance and eventually becomes negative for sufficiently negative Ri. This was found to occur for $Ri \lesssim -0.25$, where there is a mean radial outflow of fluid from the jet to the ambient.

7.2. *Application to fountains*

The boundary between the IF and OF of a fully developed fountain is defined as the location where the mean axial velocity is first equal to zero – that is, $\bar{w}(r = r_{io}) = 0$ where r_{io} is the radial location of the boundary. The IF of a fountain could then be considered an NBJ that is surrounded by an opposing shear flow, namely the OF, rather than a quiescent ambient. By integrating the conservation equations given in (7.1)–(7.4) to r_{io} instead of infinity, a system of ODEs similar to (7.5)–(7.8) can be derived that describe the IF of a fountain. In this case, we let $\tilde{r} = r_{io}$ in (3.2), (7.9) and (7.10), and all integral quantities and profile coefficients correspond to the IF:

$$\frac{\mathrm{d}Q}{\mathrm{d}z} = 2\alpha M^{1/2}, \tag{7.12}$$

$$\frac{\mathrm{d}M}{\mathrm{d}z} = \frac{FQ}{\theta_m M} - 2(r\overline{u'w'})_{r=r_{io}}, \tag{7.13}$$

$$\frac{\mathrm{d}F}{\mathrm{d}z} = -2(r\bar{u}\bar{b})_{r=r_{io}} - 2(r\overline{u'b'})_{r=r_{io}}, \tag{7.14}$$

$$\frac{\mathrm{d}}{\mathrm{d}z}\left(\gamma_m \frac{M^2}{Q}\right) = \delta_m \frac{M^{5/2}}{Q^2} + 2F. \tag{7.15}$$

The higher-order turbulence terms, i.e. turbulence components of the profile coefficients, have been neglected here. The continuity and kinetic energy equations, (7.12) and (7.15), are in the same form as (7.5) and (7.8) since $\bar{w}(r = r_{io}) = 0$, but the momentum and buoyancy equations have non-zero boundary conditions arising because $\overline{u'w'}$, $\overline{u'b'}$ and $\bar{b}$ do not go to zero at r_{io}. In the present formulation, α is related to the integral scales of the IF only, and describes the exchange of fluid between the IF and OF, where $\alpha > 0$ corresponds to fluid moving from the OF to the IF. An alternative approach may be to define the velocity scale in the definition of α in (7.9) so that it includes information about the OF velocity. However, since no assumptions are being made regarding the value or behaviour of α, any substitution here can be made valid provided that it is consistent with the conservation equations.

Similarly to the derivation of (7.11), an expression for α for the IF of a fountain may be derived using (7.12), (7.13) and (7.15) (van Reeuwijk & Craske 2015):

$$\alpha = -\frac{\delta_m}{2\gamma_m} + \left(1 - \frac{\theta_m}{\gamma_m}\right) Ri + \frac{Q}{2M^{1/2}} \frac{\mathrm{d}}{\mathrm{d}z}(\ln \gamma_m) - \frac{2Q}{M^{3/2}}(r\overline{u'w'})_{r=r_{io}}. \tag{7.16}$$

This expression differs from (7.11) only in that it includes a non-zero shear stress term at the boundary, and all integral quantities and profile coefficients are defined up to r_{io}.

Carazzo *et al.* (2010) derived a set of equations similar to (7.12)–(7.15) for the IF of a fountain, but went on to construct additional conservation equations for $\bar{w}^3$ and $\bar{w}\bar{b}$ in order to replace the boundary conditions with integral profiles, and obtained a 'confined top-hat' model for the flow. For the purposes of the present investigation, it is sufficient to derive

only the $\bar{w}^3$ equation, obtained by multiplying the momentum equation, (7.2), by $3\bar{w}^2$:

$$\frac{\partial}{\partial r}(r\bar{u}\,\bar{w}^3 + 3r\overline{u'w'}\bar{w}^2) + \frac{\partial}{\partial z}(r\bar{w}^4) = 3r\bar{w}^2\bar{b} + 6r\bar{w}\overline{u'w'}\,\frac{\partial \bar{w}}{\partial r}. \tag{7.17}$$

This may then be integrated with respect to r from zero to r_{io}, giving

$$\frac{\mathrm{d}}{\mathrm{d}z}\left(\Gamma_m \frac{M^3}{Q^2}\right) = 6\Delta_m \frac{M^{7/2}}{Q^3} + 3\mu_m \frac{MF}{\theta_m Q}, \tag{7.18}$$

which is written in terms of the new profile coefficients

$$\left.\begin{aligned} \mu_m &= \frac{1}{w_m^2 b_m r_m^2}\int_0^{\tilde{r}} \bar{w}^2\bar{b}r\,\mathrm{d}r, \\ \Gamma_m &= \frac{1}{w_m^4 r_m^2}\int_0^{\tilde{r}} \bar{w}^4 r\,\mathrm{d}r, \\ \Delta_m &= \frac{1}{w_m^4 r_m}\int_0^{\tilde{r}} \bar{w}\overline{w'u'}\,\frac{\partial \bar{w}}{\partial r}\,r\,\mathrm{d}r, \end{aligned}\right\} \tag{7.19}$$

with $\tilde{r} = r_{io}$. Note that this approach may also be applied to jets and plumes in a homogeneous environment by setting $\tilde{r} = \infty$ in the profile coefficient definitions, and integrating the conservation equations to infinity. In this case, the same expression as (7.18) is obtained.

By applying the product rule to (7.18), and using (7.12) and (7.15), a new expression for α without any boundary conditions may be derived:

$$\alpha = \frac{3}{2}\left(\frac{\delta_m}{\gamma_m} - \frac{4\Delta_m}{\Gamma_m}\right) + 3\left(\frac{\theta_m}{\gamma_m} - \frac{\mu_m}{\Gamma_m}\right)Ri + \frac{Q}{M^{1/2}}\frac{\mathrm{d}}{\mathrm{d}z}\left(\ln\frac{\Gamma_m}{\gamma_m^{3/2}}\right), \tag{7.20}$$

which is valid for arbitrary velocity and buoyancy profiles and does not make any assumptions about the self-similarity of the flow. By setting $\tilde{r} = r_{io}$ in the profile coefficient and α definition, this describes entrainment between the IF and OF of a fully developed fountain. As with (7.19), it may also be applied to jets of arbitrary buoyancy in a homogeneous environment by setting $\tilde{r} = \infty$. This is somewhat similar to the expression for α in Carazzo *et al.* (2010) (their (4.38)), which is valid for self-similar profiles and corresponds to entrainment in their top-hat model of the flow. Although both formulations are equally valid with respect to their given framework, (7.20) may be applied immediately to both the IF of a fountain or an NBJ with arbitrary profiles, using the classical integral velocity, width and buoyancy scales defined in (3.3). If the IF of the fountain were self-similar, then all profile coefficients in (7.20) would be constant, and a linear expression for α with Ri would be obtained. A linear relationship for α was also derived by Mehaddi *et al.* (2015) in their model of self-similar turbulent fountains. In their case, α and Ri were defined in terms of centreline values of the mean profiles and r_{io}, rather than integral quantities as in the present case. Although this means that the α expressions are not immediately equivalent without making additional assumptions about the shapes of the mean profiles, the linear forms of the relationships are consistent.

Both (7.16) and (7.20) are valid expressions for the entrainment coefficient of the IF of a fountain ($\tilde{r} = r_{io}$), as well for an NBJ ($\tilde{r} = \infty$). Using data from the present experiments, it is possible to calculate each of the profile coefficients present in these expressions, as

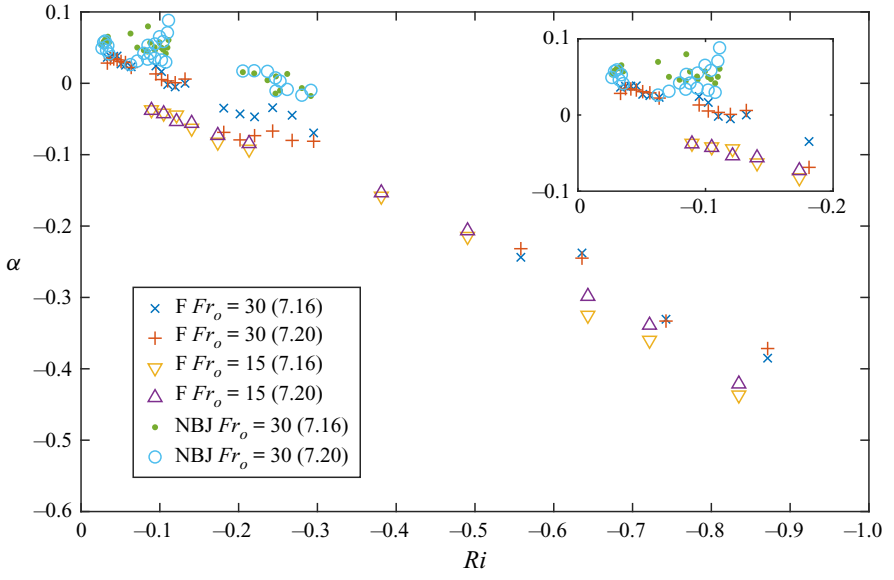

Figure 16. The entrainment coefficient, α, plotted with local Ri for the IF of an $Fr_o = 30$ and $Fr_o = 15$ fountain, and of an $Fr_o = 30$ NBJ, as calculated using (7.16) and (7.20).

well as to measure directly the boundary condition $(r\overline{u'w'})_{r=r_{io}}$ in (7.16). Figure 16 shows α calculated using both (7.16) and (7.20), for two fully developed fountains with $Fr_o = 30$ and $Fr_o = 15$, as well as for an NBJ with $Fr_o = 30$. Gaussian velocity/buoyancy profiles were assumed for the NBJ (Milton-McGurk *et al.* 2021), which results in $\gamma_m = 4/3$, $\Gamma_m = 1$, and the derivate in (7.16) and (7.20) equalling zero. For the fountain, Gaussian profiles were not assumed, though the derivative terms in these two equations were found to be negligible and so have been neglected.

As discussed in Milton-McGurk *et al.* (2021) and shown in figure 16, $\alpha < 0$ for $Ri \lesssim -0.25$ for an NBJ, indicating that there is a mean radial outflow of fluid from the jet. For the $Fr_o = 30$ fountain, α becomes negative near $Ri \simeq -0.13$, reflecting a mean outflow of fluid from the IF to the OF. For the $Fr_o = 15$ fountain, $\alpha < 0$ for the full range shown, $Ri \lesssim -0.04$. This is consistent with studies by Williamson *et al.* (2011) ($Fr_o = 7$) and Cresswell & Szczepura (1993) ($Fr_o \simeq 3.2$), who observed predominately a mean radial flow from IF to OF, other than in a small region near the source. More generally, figure 16 shows good agreement between the α estimated from (7.16), which uses a direct measurement of the IF/OF boundary condition, and that from (7.20), which uses the new profile coefficients defined in (7.19).

8. Decomposing entrainment

Turbulent entrainment is generally considered the process where fluid is transported from a non-turbulent region to a turbulent region across a turbulent/non-turbulent interface (TNTI) (e.g. Mistry *et al.* (2016)). For the NBJ, $\alpha < 0$ in figure 16 indicates that there is a mean radial outflow of fluid from the turbulent jet to the quiescent ambient. For the fully developed fountains, the size and sign of α indicate the direction and magnitude of the mean radial velocity at the interface between two turbulent regions, the IF and OF. In these contexts, α is simply a parameter constrained by the conservation equations

that is used to describe the mean radial velocity at some interface, and is therefore not necessarily a measure of 'turbulent entrainment' in the traditional sense. An NBJ with $\alpha < 0$ could undergo instantaneous 'entrainment' (i.e. flow from the ambient across the TNTI into the jet) at some times, while expelling fluid at others. For a fountain, although the IF/OF boundary is between two turbulent regions rather than a TNTI, there can still be instantaneous fluid transport across this boundary in either direction, separate from the mean flow. Such exchange of fluid across a turbulent shear layer is still often regarded as 'entrainment' (Morton 1962; McDougall 1981), and we will also take this interpretation in the context of fountains.

As discussed in Milton-McGurk *et al.* (2021), the $\alpha < 0$ in the NBJ is a natural consequence of the conservation equations, being driven primarily by the Ri term in (7.11). This term becomes increasingly negative as $Ri \to -\infty$ as the mean flow decelerates and $w_m \to 0$. For a fountain, although the return flow influences the value of α (e.g. through the boundary condition term in (7.16)), we would still expect $\alpha < 0$ and radial flow from IF to OF for sufficiently negative Ri as the IF velocity approaches zero. This section will explore an alternative approach to characterising entrainment in NBJs and fountains, where it will be separated into an inflowing 'turbulent entrainment' contribution occurring simultaneously with a mean outflow of fluid.

8.1. *Decomposed top-hat model*

Consider a control volume of a thin horizontal slice of an axisymmetric fully developed fountain, such as one taken from the fountain schematic shown in figure 1. The slice should be taken before the cap, $z < z_c$, where there are distinct IF and OF regions (e.g. $Ri \geqslant -0.5$) (Shrinivas & Hunt 2014; Hunt & Debugne 2016). For simplicity, the fountain is presumed to be orientated vertically upwards with a denser IF than OF (the opposite but equivalent case to the present experiments), and to have top-hat vertical velocity and buoyancy profiles. Here we have, for the IF and OF, $\hat{w}_{if}$ and $\hat{w}_{of}$ denoting the vertical velocities, $\hat{r}_{if}$ and $\hat{r}_{of}$ the widths, and $\hat{g}_{if} = g(\rho_a - \hat{\rho}_{if})/\rho_a$ and $\hat{g}_{of} = g(\rho_a - \hat{\rho}_{of})/\rho_a$ the buoyancies. Here, $\hat{\rho}_{if}$, $\hat{\rho}_{of}$ and ρ_a are the densities of the IF, OF and ambient, so we have $\hat{g}_{if} < 0$ and $\hat{g}_{of} < 0$. There is also a radial exchange of fluid between IF and OF that, as will be argued in the following sections, is comprised of a component resulting from turbulent entrainment and a component resulting from the buoyancy-induced spreading of the IF. These two components can, simultaneously, be in opposite directions: the turbulent component, in isolation, producing a flow from OF to IF, and the buoyant spreading component, in isolation, producing a flow from IF to OF. The combination of the two components will, depending on their balance, produce either a positive or negative net flow across the IF/OF boundary at any time. The velocity component associated with the turbulent entrainment is denoted $\hat{u}_e$, while the velocity component associated with the buoyant spreading is denoted $\hat{u}_{out}$. The equations for conservation of volume, momentum and buoyancy flux for the IF of this system are then

$$\frac{\mathrm{d}\hat{Q}_{if}}{\mathrm{d}z} = 2\hat{r}_{if}\hat{u}_e - 2\hat{r}_{if}\hat{u}_{out}, \tag{8.1}$$

$$\frac{\mathrm{d}\hat{M}_{if}}{\mathrm{d}z} = -2\hat{r}_{if}\hat{u}_e\hat{w}_{of} - 2\hat{r}_{if}\hat{u}_{out}\hat{w}_{if} + \hat{r}_{if}^2\hat{g}_{if}, \tag{8.2}$$

$$\frac{\mathrm{d}\hat{F}_{if}}{\mathrm{d}z} = 2\hat{r}_{if}\hat{u}_e\hat{g}_{of} - 2\hat{r}_{if}\hat{u}_{out}\hat{g}_{if}, \tag{8.3}$$

where $\hat{Q}_{if} = \hat{r}_{if}^2 \hat{w}_{if}$, $\hat{M}_{if} = \hat{r}_{if}^2 \hat{w}_{if}^2$ and $\hat{F}_{if} = \hat{r}_{if}^2 \hat{w}_{if} \hat{g}_{if}$ are the (scaled) volume, momentum and buoyancy fluxes.

In a fully developed fountain, the mean radial velocity is from the IF to the OF for the majority of its height. A mean radial outflow is also seen in NBJs that do not have a return flow, where it is driven by the decelerating mean flow as characterised by $Ri \to -\infty$. Despite this, there may still be instantaneous 'entrainment' from the OF to the IF of a fountain across the IF/OF interface (or from the ambient to the jet in the case of an NBJ). The present analysis will treat $\hat{u}_e$ as the 'entrainment velocity', and we will assume that it is proportional to the velocity of the IF by an entrainment coefficient, α_e:

$$\hat{u}_e = \alpha_e \hat{w}_{if}. \tag{8.4}$$

An alternative approach would be to treat α_e as instead proportional to the relative velocity difference between the IF and OF, which was also considered by Bloomfield & Kerr (2000) alongside (8.4). This approach, as well as an alternative treatment of the body-force that controls the buoyancy of the IF, is discussed in Appendix A.

No assumptions will be made about the velocity of the outflowing fluid, $\hat{u}_{out}$, which in practice is likely dependent on both IF and OF. In this formulation, even if $\hat{w}_{of} = 0$ and the flow is effectively an NBJ without a return flow, there may still be a radial outflow of fluid occurring simultaneously to entrainment (i.e. $\hat{u}_e > 0$ and $\hat{u}_{out} > 0$). This is a key difference when compared to previously proposed fountain models, such as by McDougall (1981) or Bloomfield & Kerr (2000), who modelled flow from the IF to the OF as proportional to $\hat{w}_{of}$, and related them by a second constant entrainment coefficient. The conservation equations for the present system may then be written as

$$\frac{\mathrm{d}\hat{Q}_{if}}{\mathrm{d}z} = 2\alpha_e \hat{r}_{if} \hat{w}_{if} - 2\hat{r}_{if} \hat{u}_{out}, \tag{8.5}$$

$$\frac{\mathrm{d}\hat{M}_{if}}{\mathrm{d}z} = -2\alpha_e \hat{r}_{if} \hat{w}_{if} \hat{w}_{of} - 2\hat{r}_{if} \hat{u}_{out} \hat{w}_{if} + \hat{r}_{if}^2 \hat{g}_{if}, \tag{8.6}$$

$$\frac{\mathrm{d}\hat{F}_{if}}{\mathrm{d}z} = 2\alpha_e \hat{r}_{if} \hat{w}_{if} \hat{g}_{of} - 2\hat{r}_{if} \hat{u}_{out} \hat{g}_{if}, \tag{8.7}$$

which will be referred to as the 'decomposed top-hat' model. It was mentioned previously that the system of equations could be applied to an NBJ by considering $\hat{w}_{of} = 0$, since there is no return flow. As is clear from the $\bar{w}/\bar{w}_c$ profiles for NBJs in figure 4(*b*), this is a reasonable description since the profiles go to approximately zero by $r/r_{1/2,w} \simeq 3$. However, since NBJs are subject to a net radial outflow, characterised by $\alpha < 0$ in figure 16, we should expect that $\hat{u}_{out} > \hat{u}_e$ for a portion of the flow. This ejected fluid will be negatively buoyant, implying that $\hat{g}_{of} \neq 0$ in this top-hat description of the flow. This may be counter-intuitive since NBJs do not have a fully formed OF like a fountain, so invoking a non-zero $\hat{g}_{of}$ term potentially complicates the physical interpretation of the model. For this reason, the original model described by (7.5)–(7.7) and solved in Milton-McGurk *et al.* (2021) may be more appropriate for NBJs than the top-hat description, which is presented primarily for the application to fountains. Despite this, characterising entrainment in NBJs as the balance of inflowing and outflowing fluid is still a physically meaningful description, and it is useful to compare this formulation to the original model. For this reason, we will now proceed to estimate the inflow and outflow components of entrainment with respect to the top-hat model in both fountains and NBJs using the present experimental data.

If the top-hat variables in (8.5)–(8.7) are replaced with integral quantities calculated from the experimental data, then the only unknowns in the volume and momentum flux

equations are α_e and $\hat{u}_{out}$. For the IF velocity and radius, we set $\hat{w}_{if} = w_m$ and $\hat{r}_{if} = r_m$ as defined using (3.2) and (3.3*a*,*b*) with $\tilde{r} = r_{io}$ for a fountain and $\tilde{r} = \infty$ for an NBJ. We will define the OF velocity, $\hat{w}_{of}$, similarly to w_m except that the integrals in (3.2) are evaluated from r_{io} to infinity. For the IF buoyancy scale, $\hat{g}_{if}$, one choice might be b_m from (3.3*c*), which is based on integrals of the buoyancy and velocity profiles. However, we choose instead $\hat{g}_{if} = g_m$, where g_m is defined in (8.8) (Milton-McGurk *et al.* 2020). In this definition, g_m is based on the buoyancy profile only, so is more closely related to the definition of $\hat{g}_{if}$, which is dependent only on the local density difference and gravity. If the real $\bar{w}$ and $\bar{b}$ profiles were exactly top-hat and had the same width, then b_m and g_m would be equal, where we have,

$$G = 2\int_0^{\tilde{r}} \bar{b}^2 r \,\mathrm{d}r, \quad g_m = \frac{G}{B}. \tag{8.8a,b}$$

The OF buoyancy for a fountain, $\hat{g}_{of}$, may be defined similarly to $\hat{g}_{if}$ except with the integration limits in (8.8) set from $r = r_{io}$ to infinity. The derivatives $\mathrm{d}\hat{Q}_{if}/\mathrm{d}z$ and $\mathrm{d}\hat{M}_{if}/\mathrm{d}z$ are estimated using a second-order accurate finite difference stencil. When referring exclusively to NBJs, which do not have an OF, the subscript '*if*' is omitted from the notation.

With all top-hat variables in (8.5) and (8.6) defined based on local integral scales, the pair of equations may then be solved simultaneously to obtain estimates for α_e and $\hat{u}_{out}$ along the fountain and NBJ. Figure 17 shows α_e plotted with local Ri for $Fr_o = 30$ and $Fr_o = 15$ fountains, and an $Fr_o = 30$ NBJ. Here, only results prior to the cap region are shown, since this is where the present top-hat model is expected to be valid. The entrainment coefficient for a neutral jet, which has $\hat{u}_{out} = 0$, is also shown as a horizontal line as a reference. This corresponds to $\alpha = 0.071$, as calculated using the same experimental set-up (Milton-McGurk *et al.* 2021). For the fully developed fountains, we have a slightly higher α_e in the $Fr_o = 30$ case than in the $Fr_o = 15$ case, with average values $\alpha_e = 0.062$ and $\alpha_e = 0.052$, respectively. Both fountains have $\alpha_e > 0$ over the full range shown, which contrasts to the original definition of α discussed in § 7 and shown in figure 16. This had $\alpha < 0$ for the majority of the Ri range shown ($Ri \lesssim -0.13$ for $Fr_o = 30$, and $Ri \lesssim -0.04$ for $Fr_o = 15$), and also had α generally lower in the $Fr_o = 15$ case. This previous formulation of α, which was expressed by (7.16) and (7.20), will henceforth be referred to as the 'full model'.

The results in figure 17 for the 'decomposed model' are more scattered in the NBJ since there are fewer data available, but we clearly have $\alpha_e > 0$ over the Ri range shown (with average value $\alpha_e = 0.077$). This again contrasts to the full model in figure 16, where $\alpha < 0$ for $Ri \lesssim -0.25$. Since there is no clear systematic trend for α_e with Ri in the NBJ or fountains, α_e could be approximated by taking the average value as constant. This returns values of α_e in the NBJ similar to α in a neutral jet, and fountain values somewhat lower.

In the decomposed formulation, α_e can be interpreted as a measure of the rate of 'turbulent entrainment' in the flow. For fountains, this represents 'entrainment' from the OF to the IF across the IF/OF interface, and in NBJs it is entrainment from the ambient into the jet across the TNTI. This contrasts to α in the full model shown in figure 16, which simply reflects the direction and magnitude of the mean radial velocity.

Solving (8.5) and (8.6) simultaneously also provides values for $\hat{u}_{out}$, the outflow velocity. Figure 18 shows $\hat{u}_{out}/\hat{w}_{if}$ plotted with Ri for the $Fr_o = 30$ and $Fr_o = 15$ fountains, and $Fr_o = 30$ NBJ. We see that, for all three flows, $\hat{u}_{out}$ increases with $-Ri$, and that $\hat{u}_{out} > 0$ for all $Ri < 0$. Near the source, where the IF is much stronger than the OF, $\hat{u}_{out}/\hat{w}_{if} \to 0$

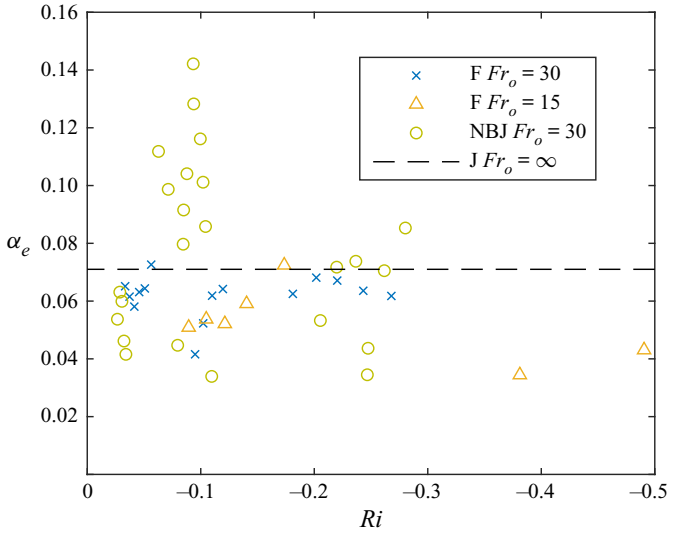

Figure 17. The entrainment coefficient, α_e, plotted with local Ri for the IF of an $Fr_o = 30$ and $Fr_o = 15$ fountain, and of an $Fr_o = 30$ NBJ. Here, $\alpha_e = \hat{u}_e/\hat{w}_{if}$, corresponding to the decomposed top-hat model described by (8.5)–(8.7). The 'standard' entrainment coefficient for the neutral jet (J), α, as reported in Milton-McGurk *et al.* (2020) using the same experimental set-up, is also shown as a reference. For neutral jets, $Ri = 0$ everywhere so α is shown as a horizontal line for clarity.

and $Ri \to 0$. This is consistent with the neutral jet case, which has $Ri = 0$ and does not have a mean outflow. Regions where there is a net radial outflow of fluid from the IF correspond to where $\hat{u}_{out} > \hat{u}_e$. Since $\alpha_e = \hat{u}_e/\hat{w}_{if}$ from (8.4), this is equivalent to where $\hat{u}_{out}/\hat{w}_{if} > \alpha_e$. Horizontal lines showing average values of α_e for the fountains and NBJ are also shown in figure 18, which therefore indicate the start of the region where there is a net radial outflow of fluid from the IF. Figure 18 therefore implies that the IFs of both Fr_o fountains and the NBJ have a net radial outflow of fluid for a large portion of their height, with the local Ri at the start of this region broadly consistent with figure 16 – that is, where $\alpha < 0$ in the original formulation given by (7.16) and (7.20).

In summary, the decomposed formulation separates radial flow between the IF and OF of a fountain into two components that are constrained by both the conservation of mass and momentum. The inflow term is described by the approximately constant α_e, which represents 'turbulent entrainment' from the OF to the IF. The outflow term, $\hat{u}_{out}/\hat{w}_{if}$, represents fluid ejected from the IF to the OF and depends on the local Ri. This term approaches zero as $Ri \to 0$ where the IF is much stronger than the OF, and increases for more negative Ri.

8.2. *Connection to the full model*

Figures 17 and 18 show that in the present decomposed top-hat formulation, the radial flow across the IF/OF boundary of a fountain (or between an NBJ and the ambient) can be described by an approximately constant turbulent entrainment coefficient, α_e, and a local Ri-dependent outflow component, $\hat{u}_{out}/\hat{w}_{if}$. If the net radial flow from the IF to the OF is denoted $\hat{u}$, so that $\hat{u} = \hat{u}_{out} - \hat{u}_e$, then the ratio $\hat{\alpha} = -\hat{u}/\hat{w}_{if}$ is a non-dimensional measure of the direction and magnitude of the mean radial flow at a given height. Using (8.4), this

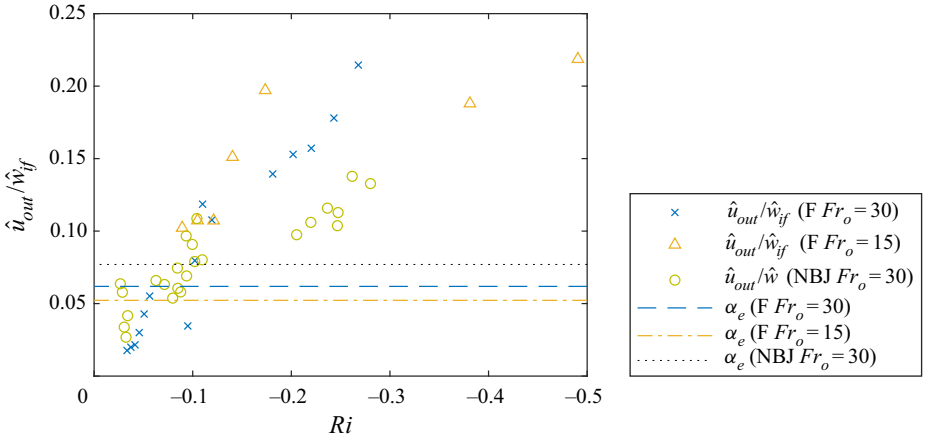

Figure 18. The normalised radial outflow velocity, $\hat{u}_{out}/\hat{w}_{if}$, with respect to the decomposed top-hat model for $Fr_o = 30$ and $Fr_o = 15$ fountains, and an $Fr_o = 30$ NBJ. Horizontal lines indicating average values of α_e from figure 17 are also shown.

may then be written as

$$\hat{\alpha} = \alpha_e - \frac{\hat{u}_{out}}{\hat{w}_{if}}, \tag{8.9}$$

which expresses $\hat{\alpha}$ as the sum of a constant and an Ri-dependent component, α_e and $-\hat{u}_{out}/\hat{w}_{if}$, respectively. This is then the present top-hat model's equivalent to α in the full model, defined by (7.11) or (7.20), which is also a measure of the mean radial velocity relative to the IF velocity scale. This equivalence may be seen by substituting (8.9) into (8.5), and recalling that the same integral definitions for $\hat{Q}_{if}$ and $\hat{M}_{if}$ are used as for Q and M in (7.5) and (7.12). If the profile coefficients in (7.20) are assumed constant, then α in the full model may be written as

$$\alpha = \frac{3}{2}\left(\frac{\delta_m}{\gamma_m} - \frac{4\Delta_m}{\Gamma_m}\right) + 3\left(\frac{\theta_m}{\gamma_m} - \frac{\mu_m}{\Gamma_m}\right) Ri, \tag{8.10}$$

which is also expressed as the sum of a constant and an Ri-dependent component, namely the first and second terms on the right-hand side of (8.10), respectively.

For Gaussian velocity and buoyancy profiles, shown in Milton-McGurk *et al.* (2021) to be a reasonable assumption in NBJs, we have that $\gamma_m = 4/3$, $\Gamma_m = 1$, $\theta_m = 2/(\lambda^2 + 1)$ and $\mu_m = 2/(2\lambda^2 + 2)$. Here, λ is defined as

$$\lambda = \frac{r_b}{r_w}, \tag{8.11}$$

where r_b and r_w are the 1/e widths of the buoyancy and velocity profiles, respectively. In Milton-McGurk *et al.* (2021), it was shown that λ, and hence θ_m and μ_m, are not constant in NBJs. However, their variation has little effect on α once multiplied by Ri, such as in (7.11) or (8.10), so they may be approximated as constant, with $\lambda \simeq 1.46$ for this purpose. For the IF of a fountain, the profiles cannot be described simply by Gaussian functions, so these profile coefficients must be estimated numerically from their integral definitions, (7.10) and (7.19). By assuming that these are constant we obtain, by taking averages, $\theta_m \simeq 0.68$ and $\mu_m \simeq 0.36$ for $Fr_o = 30$, and $\theta_m \simeq 0.65$ and $\mu_m \simeq 0.34$ for

$Fr_o = 15$. The data suggest that γ_m and Γ_m have a weak Ri dependence in fountains, with $1.27 \gtrsim \gamma_m \gtrsim 1.18$ and $0.90 \gtrsim \Gamma_m \gtrsim 0.76$ over $0 \lesssim -Ri \lesssim 0.5$. Since this variation is not very significant, these were approximated as constant using average values $\gamma_m \simeq 1.23$ and $\Gamma_m \simeq 0.85$ for $Fr_o = 30$, and $\gamma_m \simeq 1.23$ and $\Gamma_m \simeq 0.84$ for $Fr_o = 15$. All four of these profile coefficients, θ_m, μ_m, γ_m and Γ_m, therefore have similar values for both fountains, with a negligible Fr_o dependence.

For an NBJ, it was shown in Milton-McGurk *et al.* (2021) that δ_m is not constant, and instead varies linearly with Ri. The present data show that an approximately linear relation also occurs in fountains. Additionally, the profile coefficient Δ_m, defined in (7.19) and related to the turbulent production, is also well described by a linear Ri relation. These can be expressed as

$$\left.\begin{aligned} \delta_m &= \delta_o + \tilde{\delta}\, Ri, \\ \Delta_m &= \Delta_o + \tilde{\Delta}\, Ri, \end{aligned}\right\} \tag{8.12}$$

where δ_o and Δ_o represent the values at the source, and $\tilde{\delta}$ and $\tilde{\Delta}$ are additional *ad hoc* terms that capture the observed Ri dependence. The increasing of $-\delta_m$ and $-\Delta_m$ with negative Ri is related to the behaviour of the $\overline{w'u'}$ profiles discussed in Milton-McGurk *et al.* (2021) and § 3.2, where the turbulence did not decrease at the same rate as the mean flow in NBJs and fountains. A detailed analysis of the governing equations may shed light on the precise reason for this behaviour, which is left for potential future research. For the purposes of the present investigation, the observation of a linear trend and subsequent empirical expressions in (8.12) will be used.

By using these linear relations, the expression for α in (8.10) becomes

$$\alpha = \underbrace{\frac{3}{2}\left(\frac{\delta_o}{\gamma_m} - \frac{4\Delta_o}{\Gamma_m}\right)}_{P_1} + \underbrace{3\left(\frac{\theta_m}{\gamma_m} - \frac{\mu_m}{\Gamma_m} + \frac{\tilde{\delta}}{2\gamma_m} - \frac{2\tilde{\Delta}}{\Gamma_m}\right) Ri}_{P_2}. \tag{8.13}$$

This expresses α as the sum of a constant and an Ri-dependent component, P_1 and P_2, and is valid for both NBJs and fountains. The following expression, obtained by combining the linear δ_m relation with (7.20), is valid for NBJs only:

$$\alpha = \underbrace{-\frac{\delta_o}{2\gamma_m}}_{L_1} + \underbrace{\left(1 - \frac{\theta_m}{\gamma_m} - \frac{\tilde{\delta}}{2\gamma_m}\right) Ri}_{L_2}. \tag{8.14}$$

Although both (8.13) and (8.14) are equally valid for NBJs, (8.14) is simpler since it does not depend on Δ_m or Γ_m. Equation (8.14) will therefore be used for calculating α in NBJs, while (8.13) will be used for fountains. It is then useful to attempt to unify the decomposed top-hat model with the full model by considering $\hat{\alpha} = \alpha$. Both (8.13) and (8.14) express α in terms of constant and Ri-dependent components, which may then be

compared individually to the components of $\hat{\alpha}$ defined in (8.9). We would then have

$$\left.\begin{aligned} L_1 &= \alpha_e, \\ L_2 &= -\frac{\hat{u}_{out}}{\hat{w}}, \end{aligned}\right\} \text{NBJ} \tag{8.15}$$

$$\left.\begin{aligned} P_1 &= \alpha_e, \\ P_2 &= -\frac{\hat{u}_{out}}{\hat{w}_{if}}, \end{aligned}\right\} \text{Fountain} \tag{8.16}$$

for the NBJ and fountains.

These different components and their summation are given in figure 19 for the $Fr_o = 30$ NBJ, and in figure 20 for the $Fr_o = 30$ and $Fr_o = 15$ fountains. For the NBJ, figure 19(*a*) shows $L_1 = 0.075$ and $L_2 = 0.292\,Ri$ corresponding to (8.14), with the values obtained by assuming Gaussian velocity and buoyancy profiles, a constant $\lambda \simeq 1.46$, and a linear fit of δ_m (Milton-McGurk *et al.* 2021). Although very good agreement is observed between α_e and L_1, the constant component of the entrainment coefficient, there is a discrepancy between the Ri-dependent terms, L_2 and $-\hat{u}_{out}/\hat{w}$. It was found that better agreement could be obtained by including the turbulence components of the profile coefficients δ_f and γ_f in the expression for α (van Reeuwijk & Craske 2015):

$$\gamma_f = \frac{4}{w_m^3 r_m^2}\int_0^{\tilde{r}} \bar{w}\overline{w'^2} r\,\mathrm{d}r, \quad \delta_f = \frac{4}{w_m^3 r_m}\int_0^{\tilde{r}} \overline{w'^2}\,\frac{\partial \bar{w}}{\partial z}\,r\,\mathrm{d}r. \tag{8.17a,b}$$

These may be included by replacing δ_m and γ_m with $\delta_g = \delta_m + \delta_f$ and $\gamma_g = \gamma_m + \gamma_f$, wherever they appear. By initially neglecting higher-order turbulence terms in the conservation equations, (7.1)–(7.4), δ_f and γ_f were assumed negligible prior to this point. From the present NBJ data, these terms are estimated to be approximately 18 % and 35 % of the corresponding mean components, δ_m and γ_m, respectively. As a comparison, these are approximately 1 % and 25 % of the mean values for a neutral jet in the present data, and are commonly neglected for this flow (Kaminski *et al.* 2005; van Reeuwijk & Craske 2015). Now, average values $\delta_f \simeq -0.044$ and $\gamma_f \simeq 0.47$, as estimated from the present experimental data for the NBJ, will be included and assumed constant. This results in the following expression for α that can be used in place of (8.14):

$$\alpha = \underbrace{-\frac{\delta_o + \delta_f}{2\gamma_g}}_{L_1} + \underbrace{\left(1 - \frac{\theta_m}{\gamma_g} - \frac{\tilde{\delta}}{2\gamma_g}\right) Ri}_{L_2}. \tag{8.18}$$

Figure 19(*b*) then shows the same $\hat{\alpha}$ decomposition, but now with L_1 and L_2 as calculated by (8.18). Although the constant terms, α_e and L_1, are not as close as in figure 19(*a*), the agreement between the Ri terms $-\hat{u}_{out}/\hat{w}$ and L_2, and the overall summations $\hat{\alpha}$ and α, have been improved significantly. Although this supports the validity of the decomposed top-hat formulation, it raises questions as to whether the assumption made up to this point, that the turbulence components of the profile coefficients may be ignored, is appropriate. Although the turbulence components do have an effect on the entrainment rate, the modelling of NBJs in Milton-McGurk *et al.* (2021) showed that reasonable $\bar{w}_c$ agreement could nevertheless be achieved without them. It is argued therefore that neglecting these higher-order contributions is a reasonable simplification for the purposes of the

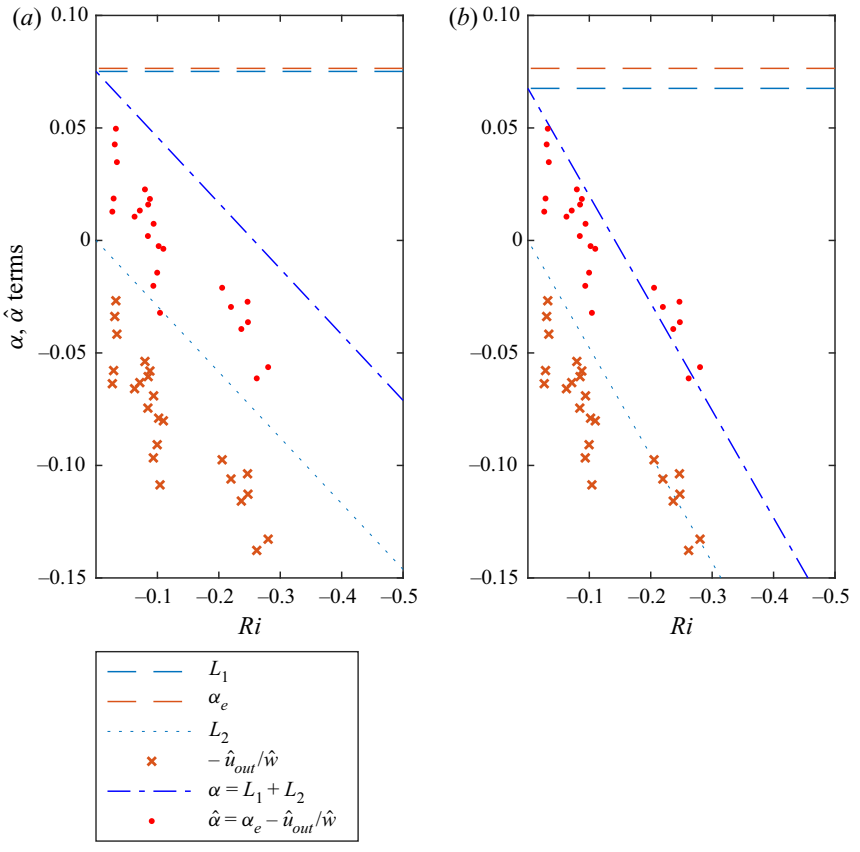

Figure 19. The constant and Ri-dependent components of the entrainment coefficient of an $Fr_o = 30$ NBJ from both the decomposed top-hat model ($\hat{\alpha} = \alpha_e - \hat{u}_{out}/\hat{w}$) and the full model ($\alpha = L_1 + L_2$). Panel ($a$) shows the terms L_1 and L_2 as calculated using (8.14), while (b) uses (8.18). That is, (a) neglects the turbulence component of profile coefficients, δ_f and γ_f, while (b) includes them.

present investigation. The effect of including additional turbulence components is left for potential future research.

The components of the entrainment coefficient for the fully developed fountain are given in figures 20(a) and 20(b) for the $Fr_o = 30$ and 15 cases, respectively. For both Fr_o cases, (8.13) has been used to calculate the α components, P_1 and P_2, with the turbulence profile coefficients neglected. Here, the linear fits used to obtain $\delta_m = \delta_o + \tilde{\delta}\, Ri$ and $\Delta_m = \Delta_o + \tilde{\Delta}\, Ri$ have been obtained from the experimental data for each Fr_o fountain separately. The $Fr_o = 30$ case in figure 20(a) shows good agreement between the constant and Ri-dependent components, with $\alpha_e \simeq P_1$ and $-\hat{u}_{out}/\hat{w}_{if} \simeq P_2$, and subsequently $\alpha \simeq \hat{\alpha}$. Although the agreement is more modest in the $Fr_o = 15$ case, the components and their summation are still broadly consistent.

In the case of the NBJ, the constant component corresponds to turbulent entrainment from ambient fluid into the NBJ. Near the source where $Ri \to 0$, this fully describes entrainment and may be interpreted as the 'neutral jet' value. This is supported by the present experimental data, which give similar values of $\alpha = 0.071$ and $\alpha_e = 0.077$ for the neutral and negatively buoyant jets, respectively. For a fully developed fountain, the constant component can be interpreted as describing the 'turbulent entrainment' from the

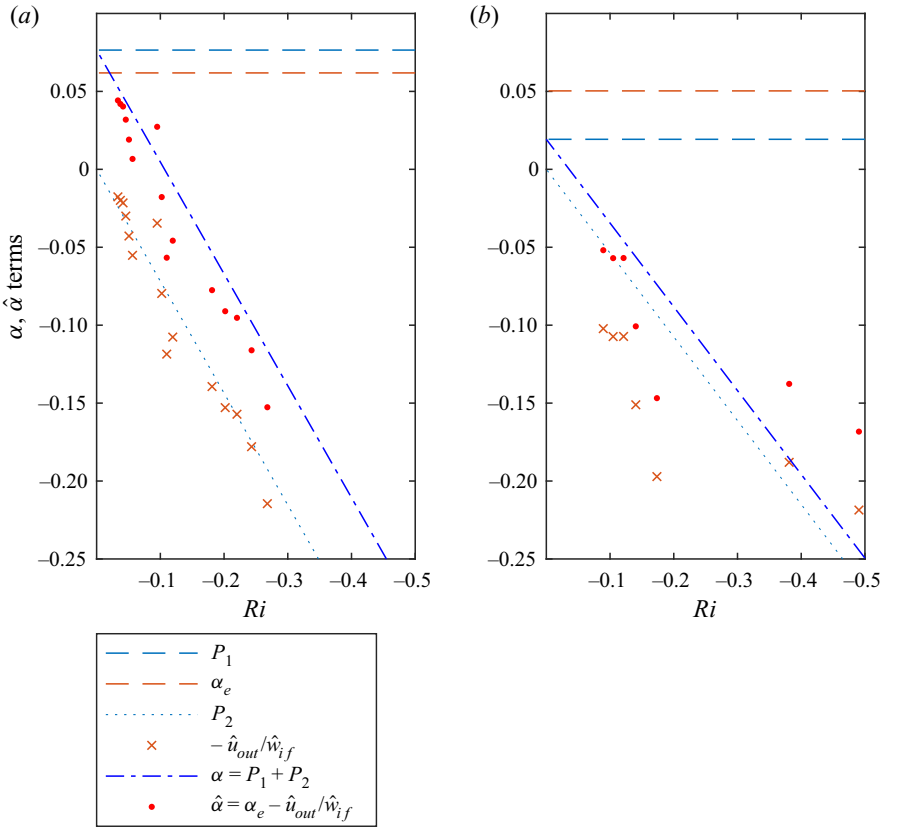

Figure 20. The constant and Ri-dependent components of the entrainment coefficient of a fully developed fountain from both the decomposed top-hat model ($\hat{\alpha} = \alpha_e - \hat{u}_{out}/\hat{w}$) and the full model ($\alpha = L_1 + L_2$). Results for the $Fr_o = 30$ fountain are shown in (a), and for the $Fr_o = 15$ case in (b).

OF to the IF associated with the mean IF velocity. In this case, the values are slightly lower than the neutral/negatively buoyant jets, and also have a source Fr_o dependence, with $\alpha_e \simeq 0.062$ and $\alpha_e \simeq 0.052$ for the $Fr_o = 30$ and 15 cases, respectively. This difference may be attributed to the existence of a return flow, which will depend on Fr_o and is still present even at the source where $Ri = 0$.

In describing the radial flow between the IF and OF of a fountain, the highly simplified decomposed top-hat description of a fountain is consistent with the the more general full model approach discussed in § 7.2. This is also applicable to an NBJ, which can be thought of as a fountain with a zero-velocity OF under the same top-hat formulation. This provides evidence that despite fountains generally having a mean radial flow from the IF to the OF (or into the ambient for an NBJ), they still 'entrain' fluid at a rate proportional to their characteristic axial velocity. This entrainment is captured by α_e in the top-hat model, and by terms L_1 and P_1 in the full model.

While buoyant jets and plumes are subject to an acceleration due to their positive buoyancy and $Ri > 0$, NBJs are instead decelerated as characterised by their increasingly negative Ri. This has implications for entrainment as captured by the $\hat{u}_{out}$ term in the decomposed formulation, and by L_2 and P_2 in the full model. In NBJs under the decomposed formulation, this has the effect of encouraging a radial outflow of fluid.

In a physical flow, there will be instantaneous entrainment at some times and radial outflow at others. A mean radial outflow of fluid then occurs when the *Ri*-dependent term is larger in magnitude than the constant entrainment term, resulting in $\alpha < 0$. In addition to the present experiments, different regions of mean radial inflow and outflow have also been observed in other fountain investigations, such as by Williamson *et al.* (2011) and Cresswell & Szczepura (1993). The present decomposed top-hat model provides a consistent description of this observation, allowing it to be understood in a context similar to that for the classical entrainment relations applied originally to jets and plumes.

8.3. *Special cases: pure jets/plumes*

It is also useful to consider more closely the application of these models to neutral jets and plumes. Once fully developed, these idealised flows can be considered fully self-similar with constant profile coefficients. By assuming additionally that the velocity and buoyancy/scalar profiles are Gaussian, (7.11) and (7.20) become

$$\alpha = -\frac{3}{8}\delta_m + \left(1 - \frac{3}{2(\lambda^2+1)}\right) Ri, \tag{8.19}$$

$$\alpha = \frac{3}{2}\left(\frac{3}{4}\delta_m - 4\Delta_m\right) + 3\left(\frac{3}{2(\lambda^2+1)} - \frac{2}{2\lambda^2+1}\right) Ri, \tag{8.20}$$

where λ is the ratio of 1/e widths of the scalar and velocity profiles. For a neutral jet, $Ri = 0$, so by equating (8.20) and (8.19), we find that $\delta_m = 4\Delta_m$. This is supported by the experimental data for a neutral jet (Milton-McGurk *et al.* 2021), where we find $\delta_m \simeq 4\Delta_m \simeq -0.20$.

If a self-similar buoyant jet or pure plume is now considered, with $0 < Ri \leqslant Ri_p$ and constant δ_m, then by equating the *Ri* components of (8.19) and (8.20), we obtain

$$\frac{6}{\lambda^2+1} - \frac{6}{2\lambda^2+1} - 1 = 0, \tag{8.21}$$

that is, a non-linear equation restricting the possible values of λ to maintain consistency between (8.20) and (8.19), with positive solutions $\lambda = 1$ and $\lambda = 1/\sqrt{2}$. Under these assumptions, we then have that λ can take only the values 1 and $1/\sqrt{2}$ in order to maintain consistency with the conservation of mass, momentum and kinetic energy equations, (7.1)–(7.4), and the additionally derived $\bar{w}^3$ equation in (7.17). Although, to the best of the authors knowledge, there have been no studies to have reported a value as low as $\lambda = 1/\sqrt{2} \simeq 0.707$ in buoyant jets or plumes, the prediction $\lambda = 1$ is remarkably consistent with the existing plume literature (Papanicolaou & List 1988; Shabbir & George 1994; Wang & Law 2002; van Reeuwijk *et al.* 2016). This then provides a new theoretical justification of the commonly reported $\lambda = 1$ observation in pure plumes. It should be noted that although this consistency requirement exists for plumes/buoyant jets under these assumptions, there is no constraint here on λ in neutral jets ($Ri = 0$), which are typically reported to have $1.15 \lesssim \lambda \lesssim 1.30$ (Fischer *et al.* 1979; Wang & Law 2002; Ezzamel, Salizzoni & Hunt 2015). If δ_m is not constant, such as in NBJs or near the source in positively buoyant jets (van Reeuwijk *et al.* 2016), then (8.21) is also not valid.

Consider now the application of the decomposed top-hat model to a Gaussian neutral jet by equating $\alpha = \hat{\alpha}$ from (8.19) and (8.9). Here, the *Ri*-dependent term is zero and we have $\alpha_e = -3\delta_m/8$ – that is, a constant turbulent entrainment coefficient α_e, and no

outflow term. This is consistent with the classical description of a turbulent jet, which entrains ambient fluid at a rate proportional to its mean axial velocity, and is not subject to any 'mean radial outflow'.

For a buoyant jet with $\lambda = 1$ and constant δ_m, by setting $\alpha = \hat{\alpha}$ we obtain

$$\alpha = \alpha_e - \frac{\hat{u}_{out}}{\hat{w}} = -\tfrac{3}{8}\delta_m + \tfrac{1}{4}Ri. \tag{8.22}$$

Equating the constant and Ri-dependent terms would then give $\alpha_e = -3\delta_m/8$ and $-\hat{u}_{out}/\hat{w} = Ri/4$. We then have $-\hat{u}_{out}/\hat{w} > 0$ and $\alpha_e > 0$, that is, both terms promoting entrainment from the ambient into the plume, rather than a balance of inflow and outflow as is the case in an NBJ. If applying the decomposed top-hat formulation to positively buoyant jets or plumes, it is therefore potentially misleading to refer to the Ri-dependent term as the 'outflow term', $\hat{u}_{out}$. Despite this, it is still a consistent description of the flow, and distinguishes between radial inflow associated with turbulent entrainment and that associated with positive buoyancy. In these applications, it may simply be preferable to use an alternative nomenclature, such as replacing $\hat{u}_{out}$ with $\hat{u}_b$ to indicate that it is radial flow associated with buoyancy.

9. Model predictions

The predictions of the decomposed top-hat model presented in § 8.1 are now compared to the present experimental data for the $Fr_o = 15$ and 30 fully developed fountains. As discussed in §§ 8.1 and 8.2, in practice the full model is more appropriate for NBJs (Milton-McGurk *et al.* 2021), since this does not require characterising $\hat{g}_{of}$ separately, so only the fountain cases are pursued here. The model corresponds to the system of equations (8.5)–(8.7), which are are solved numerically using a constant $\alpha_e = 0.052$ and 0.062 for the $Fr_o = 15$ and 30 fountains, respectively, and linear empirical fits for the OF terms $\hat{w}_{of}$ and $\hat{g}_{of}$, and the radial outflow term $\hat{u}_{out}$. Since we do not have data for these terms near the source, the model is solved from $z/D = 9.8$ and 13.5 for the $Fr_o = 15$ and 30 fountains, respectively. Figures 21(*a*)–21(*c*) show the data and model predictions for $\hat{w}_{if}$, $\hat{r}_{if}$ and $\hat{g}_{if}$. Good agreement is obtained for the velocity scale for both Fr_o fountains for the full z/D range shown, and good agreement for the width scale until approximately the start of the cap region, where the model is not expected to be valid. The buoyancy prediction for the $Fr_o = 30$ fountain agrees well with the data, while the $Fr_o = 15$ prediction is less favourable.

The process of solving the model to produce the predictions shown in figure 21 involved assuming a constant α_e and a linear fit of $\hat{u}_{out}$, and then solving (8.5)–(8.7) for $\hat{Q}_{if}$, $\hat{M}_{if}$ and $\hat{F}_{if}$. The values of α_e and $\hat{u}_{out}$ were calculated originally in § 8 from the same system of equations, except using the present data for $\hat{Q}_{if}$, $\hat{M}_{if}$ and $\hat{F}_{if}$, and solving for unknowns α_e and $\hat{u}_{out}$. Any discrepancy between the data and predictions of the model must therefore be attributed to the assumptions made when solving the ODEs for $\hat{Q}_{if}$, $\hat{M}_{if}$ and $\hat{F}_{if}$, which were not present when solving originally for α_e and $\hat{u}_{out}$. This includes the assumption of a constant α_e and a linear fit for $\hat{u}_{out}$. Figures 17 and 18 both show more scatter in the data for α_e and $\hat{u}_{out}$ for the $Fr_o = 15$ fountain than for $Fr_o = 30$, which may help to explain the reduced agreement in the $Fr_o = 15$ case. The assumption of a constant α_e, while appropriate for the $Fr_o = 30$ case, may therefore be less valid for the lower Fr_o flow.

Although figure 21 shows that the model makes very good $\hat{w}_{if}$, $\hat{r}_{if}$ and $\hat{g}_{if}$ predictions for the $Fr_o = 30$ fountain, and good $\hat{w}_{if}$ and $\hat{r}_{if}$ predictions for the $Fr_o = 15$ case, knowledge of the OF is required. This is captured through the terms $\hat{w}_{of}$ and $\hat{g}_{of}$, and $\hat{u}_{out}$, which

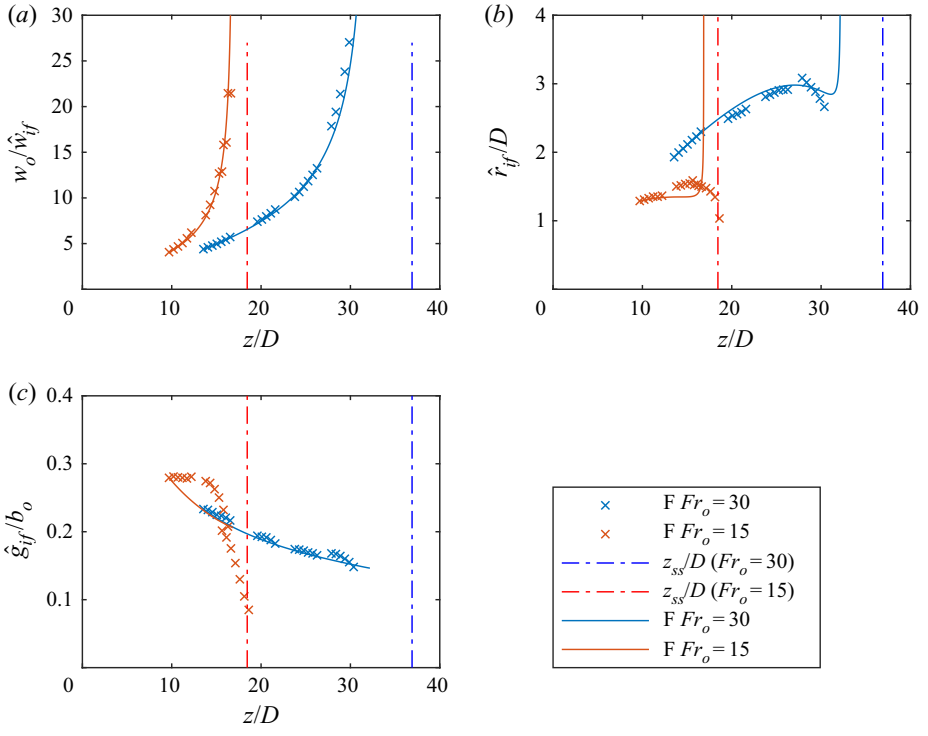

Figure 21. Predictions of the decomposed top-hat model described by (8.5)–(8.7) alongside experimental data for the $Fr_o = 15$ and 30 fountains. The velocity scale, $\hat{w}_{if}$, is given in (*a*), the radius scale, $\hat{r}_{if}$, in (*b*), and the buoyancy scale, $\hat{g}_{if}$, in (*c*), all normalised by source quantities.

vary with axial location and depend on Fr_o. Further research may seek to model explicitly the OF, as well as the cap region, using a similar decomposed formulation (i.e. one that does not assume a constant $\hat{u}_{out}/\hat{w}_{if}$). However, even if the OF is successfully modelled, knowledge of α_e and $\hat{u}_{out}$ is still required for a given Fr_o fountain. Future studies may therefore seek to formulate a model that can describe the radial flow between the IF and OF that avoids the need for Fr_o-dependent empirical terms.

10. Conclusion

Fully developed fountains, with an established IF/OF structure, have been investigated using velocity and buoyancy measurements obtained from combined PIV and PLIF experiments. We have aimed to explore the extent to which the IF of a fountain is similar to an NBJ, which does not have a return flow, and thus reveal the effect of the OF on the IF in high Fr_o fountains. Mean and turbulence profiles for fountains and NBJs at similar local Fr were presented in §§ 3.1 and 3.2. Unlike NBJs, the mean $\bar{w}$ and $\bar{c}$ profiles in fountains do not collapse when normalised by their local centreline value and respective half-widths across the full width of the profiles, so are not self-similar in this sense. This is consistent with previous studies that have also obtained data on the internal velocity/scalar fields (Mizushina *et al.* 1982; Cresswell & Szczepura 1993; Williamson *et al.* 2011). Despite this, the profiles collapse reasonably well in the IF for $r \lesssim r_{1/2,w}$ and $r \lesssim r_{1/2,c}$ over the range of axial locations investigated ($14 \lesssim z/D \lesssim 28$, $1.25 \lesssim Fr \lesssim 5.47$), with the profile differences being largest in the OF. Both the NBJ and IF of the fountain have $\overline{w'u'}/\bar{w}_c^2$

and $\overline{w'^2}/\bar{w}_c^2$ profiles that increase with axial distance, which is due primarily to the mean flow, characterised by $\bar{w}_c$, decreasing at a greater rate than the turbulence quantities. The magnitudes of these profiles are considerably larger in the fountain than in the NBJ at similar Fr, likely due to interactions between the IF and OF resulting in an increase in turbulence in the IF. When considering the $\bar{w}$ and $\bar{c}$ profiles of fountains with different Fr_o at locations where the local Fr values were similar, the profiles collapsed approximately for $r \lesssim r_d$, the location of 'maximum return flow'. This suggests that for $r \lesssim r_d$, the mean profiles of a fountain are well characterised by the mean local integral scales for the IF, captured here by Fr. This was not the case for the turbulence quantities, such as $\overline{w'u'}/\bar{w}_c^2$ and $\overline{u'c'}/\bar{w}\,\bar{c}$ in figure 12, where there is a clear Fr_o dependence on both the shape and magnitude of the profiles. In $Fr_o = 10$ and 30 NBJs, these profiles were similar at locations of similar Fr. The difference in the two fountains is therefore attributed to the effect of the OF at a particular Fr location, and contributes to differences in entrainment in different Fr_o fountains.

Another aim of this study was to investigate the extent to which entrainment in the IF of fountains is affected by the turbulent OF. This was pursued in §§ 7 and 8, where entrainment between the IF and OF in fountains is compared to entrainment between an NBJ and a quiescent ambient. An expression for the entrainment coefficient valid for both fountains and NBJs, as well as neutral/positively buoyant jets and plumes, was derived and presented in (7.20). Along with (7.16), this was used to estimate α in fountains and NBJs in figure 16, showing a strong Ri dependence on entrainment in both flows. For both fountains, $\alpha < 0$ over a large portion of their height, a finding consistent with previous studies by Williamson *et al.* (2011) ($Fr_o = 7$) and Cresswell & Szczepura (1993) ($Fr_o = 3.2$).

An alternative formulation of entrainment, the 'decomposed top-hat model' was introduced in § 8, where α is split into inflow and outflow components, α_e and $\hat{u}_{out}/\hat{w}_{if}$. These were estimated along the fountains and NBJ using the present experimental data, finding that α_e was approximately constant whilst $\hat{u}_{out}/\hat{w}_{if}$ varied with Ri. This formulation was shown to be broadly consistent with a simplified version of the 'full model' in § 8.2, where entrainment can also be expressed as the sum of a constant and an Ri-dependent component. These depend on the dimensionless turbulence production terms δ_m and Δ_m, which vary with Ri in both NBJs and fountains. Despite NBJs and fountains generally having a non-constant α, the decomposed top-hat formulation provides an interpretation of entrainment that is similar to the classical jet and plume description used by Morton *et al.* (1956) – that is, that turbulent entrainment can be expressed by a characteristic velocity at that height multiplied by a constant entrainment coefficient. However, for an NBJ or fountain IF, there is also an Ri-dependent radial outflow arising due to the flow's (negative) buoyancy.

The present study has found certain similarities between NBJs without a return flow and fully developed fountains. These include turbulence profiles that increase with axial location due to a strongly decelerating mean flow, and a non-constant entrainment coefficient that reverses sign after some distance. The entrainment coefficient in the $Fr_o = 15$ fountain is consistently lower than in the $Fr_o = 30$ case, although both are approximately linear with Ri. This apparent Fr_o dependence on α likely arises due to differences in the OF in these fountains, and presents a challenge for predicting accurately entrainment for arbitrary Fr_o fountains. Future research may seek to develop a description of the local, Ri-dependent, entrainment in fountains that can more easily be applied to different Fr_o cases. Such a study would likely involve more directly modelling of the OF,

and could benefit from additional internal velocity/scalar measurements along the fountain for a greater range of Fr_o. The present study has also focused primarily on entrainment between the IF and OF of a fountain, whereas future research may seek to investigate it between the ambient and OF, including in the cap region.

Funding. The support of the Australian Research Council for this project is gratefully acknowledged.

Declaration of interests. The authors report no conflict of interest.

Author ORCIDs.
L. Milton-McGurk https://orcid.org/0000-0002-4294-729X;
N. Williamson https://orcid.org/0000-0001-7246-8356;
M.P. Kirkpatrick https://orcid.org/0000-0002-7157-6440.

Appendix A. Alternative entrainment and body-force formulations

The decomposed model presented in § 8.1 describes radial flow from the OF to the IF as proportional to the IF velocity, as implied by the definition of α_e in (8.4). This was the entrainment formulation used by Hunt & Debugne (2016) and also considered by Bloomfield & Kerr (2000) in their theoretical models of a fountain, and will be referred to as E1. McDougall (1981) used an alternative formulation, which was also considered by Bloomfield & Kerr (2000), where $\hat{u}_e$ is instead proportional to the relative velocity difference between the IF and OF. In this case, the entrainment coefficient in (8.4) would be defined using the substitution

$$\hat{u}_e = \alpha_e(\hat{w}_{if} + \hat{w}_{of}), \tag{A1}$$

which will be referred to as E2, the second entrainment formulation. Note that the positive sign in front of $\hat{w}_{of}$ corresponds to the positive downward direction of $\hat{w}_{of}$ implied by figure 1.

Another way in which the fountain model could be modified is to consider alternative body-force formulations. McDougall (1981) considered two formulations. The first was that the buoyancy force acting on the IF depends on the density difference between the IF and the ambient fluid. This follows from the assumption that the pressure is hydrostatic everywhere and that lines of constant pressure are horizontal. This will be referred to as B1, and was the formulation used in § 8.1 in the momentum equations (8.2) and (8.6). The second body-force formulation considered by McDougall (1981), and also by Bloomfield & Kerr (2000) and Hunt & Debugne (2016), is to treat the OF as an effective 'ambient' with respect to the IF. The buoyancy force acting on the IF would then be related to the density difference between the IF and OF. This body-force formulation will be denoted B2, and results in an alternative momentum equation for the IF,

$$\frac{\mathrm{d}\hat{M}_{if}}{\mathrm{d}z} = -2\hat{r}_{if}\hat{u}_e\hat{w}_{of} - 2\hat{r}_{if}\hat{u}_{out}\hat{w}_{if} + \hat{r}_{if}^2\left(\hat{g}_{if} - \hat{g}_{of} + \hat{w}_{of}\frac{\mathrm{d}\hat{w}_{of}}{\mathrm{d}z}\right), \tag{A2}$$

which would replace (8.2) (McDougall 1981; Bloomfield & Kerr 2000; Hunt & Debugne 2016). Here, the third term in parentheses, $\hat{w}_{of}\,\mathrm{d}\hat{w}_{of}/\mathrm{d}z$, arises due to the accelerating reference frame (i.e. the OF) (McDougall 1981).

There are then four combinations of entrainment and body-force formulations, each of which were considered by Bloomfield & Kerr (2000), and which can be expressed as B1E1, B1E2, B2E1 and B2E2. Bloomfield & Kerr (2000) also used entrainment relations to describe radial flow from the IF to the OF, and from the ambient to the IF, and assumed constant entrainment coefficients. By combining these with a system of equations similar

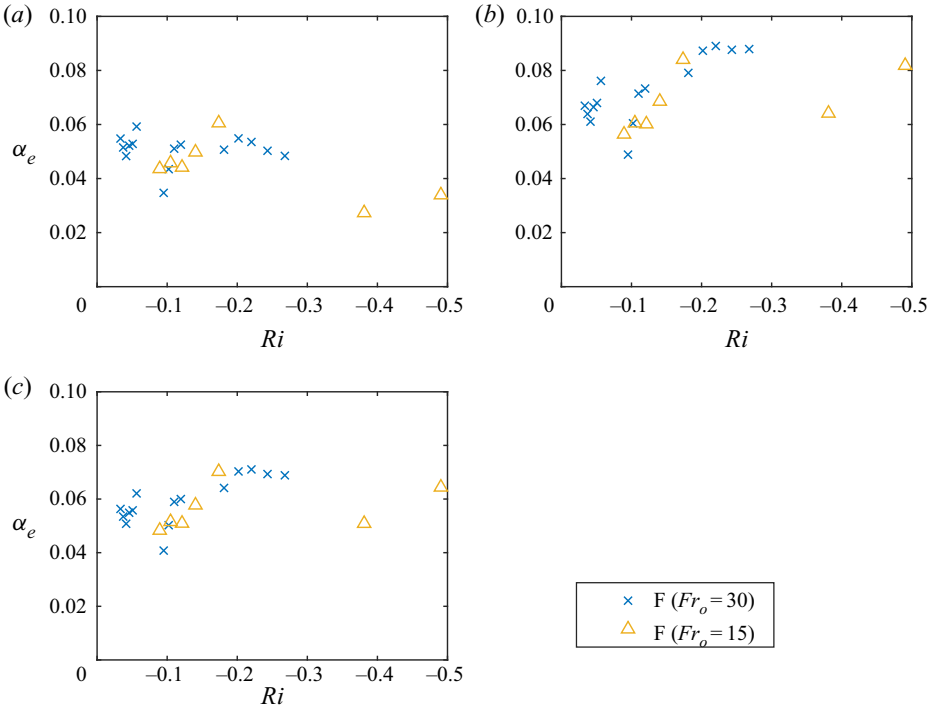

Figure 22. The entrainment coefficient, α_e, for (*a*) B1E2, (*b*) B2E1, and (*c*) B2E2, for $Fr_o = 15$ and 30 fountains under the decomposed top-hat model, as estimated from the present experimental data.

	B1E1	B1E2	B2E1	B2E2
α_e ($Fr_o = 15$)	0.052	0.044	0.068	0.056
α_e ($Fr_o = 30$)	0.062	0.051	0.073	0.059

Table 2. Mean values of α_e for $Fr_o = 15$ and 30 fountains in the decomposed top-hat model for the alternative body-force and entrainment formulations, as estimated from the present experimental data.

to (8.1)–(8.3) but for the OF, they solved their fountain model for the four formulations. In the present study, instead, we have used experimental data to estimate the inflow entrainment coefficient, α_e, and outflow component, $\hat{u}_{out}$, without making any further assumptions. Figures 17 and 18, and the discussion in § 8.1, correspond to this approach applied to formulation B1E1.

The same procedure is now applied to the remaining three entrainment/body-force formulations, B1E2, B2E1 and B2E2 – that is, solving simultaneously conservation equations (8.1) and either (8.2) or (A2), while using either entrainment relation for $\hat{u}_e$, to calculate α_e and $\hat{u}_{out}$ at a range of axial locations along the fountain. The value of α_e for these formulations is plotted with Ri in figures 22(*a–c*). Similarly to figure 17 corresponding to B1E1, α_e is reasonably constant in each formulation with no significant trend with Ri. The mean α_e value for each case is summarised in table 2, which shows the largest values in B2E1, and consistently higher values in the $Fr_o = 30$ fountain than in the $Fr_o = 15$ fountain.

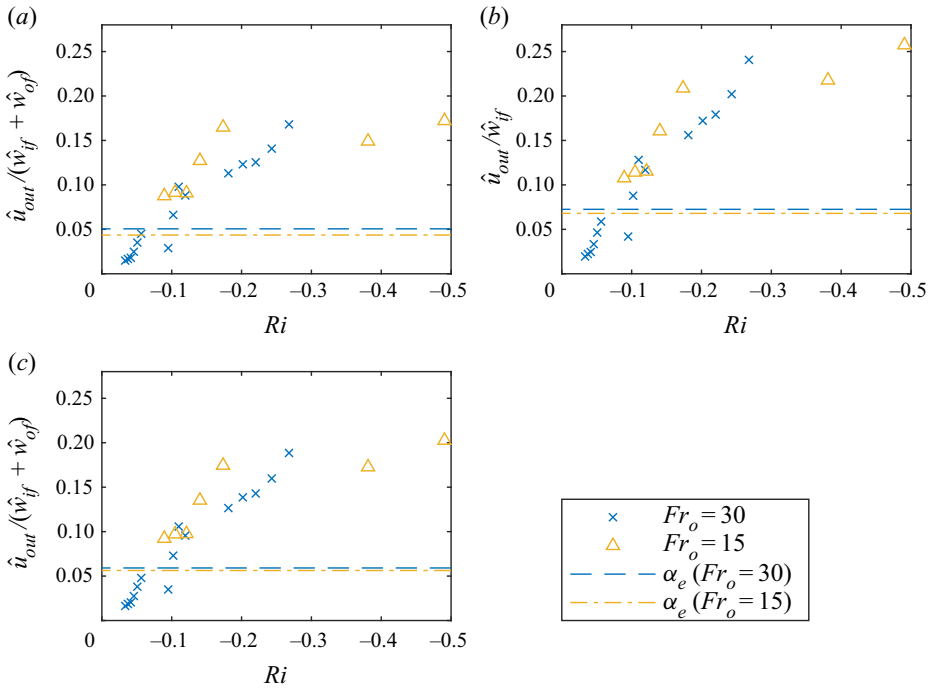

Figure 23. The radial velocity outflow component, $\hat{u}_{out}$, for (*a*) B1E2, (*b*) B2E1, and (*c*) B2E2, for $Fr_o = 15$ and 30 fountains under the decomposed top-hat model, as estimated from the present experimental data. In each case, $\hat{u}_{out}$ is normalised so that it is consistent with the definition of α_e.

While the value of the outflow component, $\hat{u}_{out}$, is affected by the body-force formulation, it is independent of the choice of α_e substitution when solving simultaneously the conservation of volume and momentum equations using the present data. For example, the conservation equations could be solved simultaneously for $\hat{u}_e$ and $\hat{u}_{out}$ before substituting in the chosen entrainment relation, resulting in the same value of $\hat{u}_{out}$ for E1 and E2. However, when comparing with α_e, it is useful to normalise $\hat{u}_{out}$ in a way that is consistent with the definition of α_e. For example, in B1E2, $\alpha_e = \hat{u}_e/(\hat{w}_{if} + \hat{w}_{of})$, so it is useful to consider $\hat{u}_{out}/(\hat{w}_{if} + \hat{w}_{of})$. The normalised outflow component is presented in figure 23 for B1E2, B2E1 and B2E2, along with horizontal lines corresponding to the mean α_e value to indicate the start of the region where there is a net radial outflow from the IF to the OF (since this occurs when $\hat{u}_{out} > \hat{u}_e$). Similarly to figure 18, all cases show that the normalised outflow component is strongly dependent on *Ri*. The precise values differ slightly for each entrainment/body-force formulation, but are nevertheless broadly similar.

McDougall (1981) and Bloomfield & Kerr (2000) assumed that the radial outflow component was proportional to the OF velocity by a constant entrainment coefficient when solving their fountain models. In the present case, it was desirable to formulate a model that was also compatible with NBJs, which have $\hat{w}_{of} = 0$ but can still be subject to a net radial outflow. In this case, an entrainment relation that assumes $\hat{u}_{out} \sim \hat{w}_{of}$ is not well defined and so has not been considered until now. Despite this, we now briefly consider $\hat{u}_{out}/\hat{w}_{of}$ for the two body-force formulations in the $Fr_o = 15$ and 30 fountains, shown in figure 24, recalling that the value of $\hat{u}_{out}$ is the same in both entrainment formulations. Figure 24 shows a strong *Ri* dependence on $\hat{u}_{out}/\hat{w}_{of}$, with broadly similar values for both

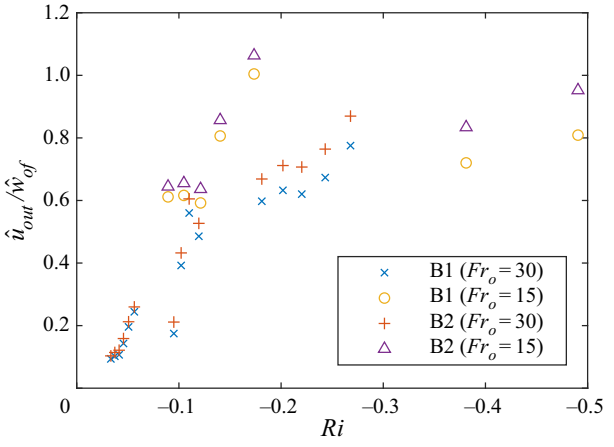

Figure 24. The radial velocity outflow component, $\hat{u}_{out}$, normalised by the OF velocity, $\hat{w}_{of}$, for $Fr_o = 15$ and 30 fountains under the decomposed top-hat model.

body-force formulations for each Fr_o fountain. Bloomfield & Kerr (2000) assumed that this quantity was a constant equal to $\hat{u}_{out}/\hat{w}_{of} = 0.147$, which is similar to the present values near $Ri \simeq -0.05$, but lower than those further along the fountain.

Although the precise values of α_e are affected by the choice of body-force and entrainment formulations, and $\hat{u}_{out}$ by the choice of body-force formulation only, the overall trends for both quantities are very similar – that is, the Ri dependence of the outflow component shown in figures 23 and 24, and the approximately constant α_e in figure 22 and table 2. The arguments put forward in § 8.1 corresponding to B1E1 may therefore also be applied to the other formulations, namely, that the approximately constant α_e can be interpreted as representing 'turbulent entrainment' from the OF to the IF, similar to the classical description of entrainment in pure jets and plumes (Morton *et al.* 1956). The outflow component then represents the fluid ejected from the IF to the OF as a result of the decelerating and expanding IF, as well as capturing other complex interactions with the OF. Although all four formulations are similar in this way, the B1E1 formulation most closely resembles the 'full model' discussed in § 7, which relates α to IF quantities only. For this reason, we considered B1E1 primarily in this investigation, and all references to the 'decomposed top-hat model' outside this appendix correspond to this formulation.

References

Bloomfield, L.J. & Kerr, R.C. 2000 A theoretical model of a turbulent fountain. *J. Fluid Mech.* **424**, 197–216.

Burridge, H.C. & Hunt, G.R. 2012 The rise heights of low- and high-Froude-number turbulent axisymmetric fountains. *J. Fluid Mech.* **691**, 392–416.

Burridge, H.C. & Hunt, G.R. 2016 Entrainment by turbulent fountains. *J. Fluid Mech.* **790**, 407–418.

Carazzo, G., Kaminski, E. & Tait, S. 2006 The route to self-similarity in turbulent jets and plumes. *J. Fluid Mech.* **547**, 137–148.

Carazzo, G., Kaminski, E. & Tait, S. 2008 On the rise of turbulent plumes: quantitative effects of variable entrainment for submarine hydrothermal vents, terrestrial and extra terrestrial explosive volcanism. *J. Geophys. Res.: Solid* **113** (B9), B09201.

Carazzo, G., Kaminski, E. & Tait, S. 2010 The rise and fall of turbulent fountains: a new model for improved quantitative predictions. *J. Fluid Mech.* **657**, 265–284.

Cresswell, R.W. & Szczepura, R.T. 1993 Experimental investigation into a turbulent jet with negative buoyancy. *Phys. Fluids* A **5** (11), 2865–2878.

DELLINO, P., *et al.* 2014 Volcanic jets, plumes, and collapsing fountains: evidence from large-scale experiments, with particular emphasis on the entrainment rate. *Bull. Volcanol.* **76** (6), 834.
EZZAMEL, A., SALIZZONI, P. & HUNT, G.R. 2015 Dynamical variability of axisymmetric buoyant plumes. *J. Fluid Mech.* **765**, 576–611.
FISCHER, H.B., LIST, J.E., KOH, C.R., IMBERGER, J. & BROOKS, N.H. 1979 *Mixing in Inland and Coastal Waters*. Academic.
FOX, D.G. 1970 Forced plume in a stratified fluid. *J. Geophys. Res.* **75** (33), 6818–6835.
HUNT, G.R. & BURRIDGE, H.C. 2015 Fountains in industry and nature. *Annu. Rev. Fluid Mech.* **47**, 195–220.
HUNT, G.R. & DEBUGNE, A.L.R. 2016 Forced fountains. *J. Fluid Mech.* **802**, 437–463.
HUSSEIN, H.J., CAPP, S.P. & GEORGE, W.K. 1994 Velocity measurements in a high-Reynolds-number, momentum-conserving, axisymmetric, turbulent jet. *J. Fluid Mech.* **258**, 31–75.
KAMINSKI, E., TAIT, S. & CARAZZO, G. 2005 Turbulent entrainment in jets with arbitrary buoyancy. *J. Fluid Mech.* **526**, 361–376.
KAYE, N.B. & HUNT, G.R. 2006 Weak fountains. *J. Fluid Mech.* **558**, 319–328.
MCDOUGALL, T.J. 1981 Negatively buoyant vertical jets. *Tellus* **33** (3), 313–320.
MEHADDI, R., VAUX, S., CANDELIER, F. & VAUQUELIN, O. 2015 On the modelling of steady turbulent fountains. *Environ. Fluid Mech.* **15** (6), 1115–1134.
MILTON-MCGURK, L., WILLIAMSON, N., ARFMFIELD, S.W., KIRKPATRICK, M.P. & TALLURU, K.M. 2021 Entrainment and structure of negatively buoyant jets. *J. Fluid Mech.* **911**, A21.
MILTON-MCGURK, L., WILLIAMSON, N., ARMFIELD, S.W. & KIRKPATRICK, M.P. 2020 Experimental investigation into turbulent negatively buoyant jets using combined PIV and PLIF measurements. *Intl J. Heat Fluid Flow* **82**, 108561.
MISTRY, D., PHILIP, J., DAWSON, J.R. & MARUSIC, I. 2016 Entrainment at multi-scales across the turbulent/non-turbulent interface in an axisymmetric jet. *J. Fluid Mech.* **802**, 690–725.
MIZUSHINA, T., OGINO, F., TAKEUCHI, H. & IKAWA, H. 1982 An experimental study of vertical turbulent jet with negative buoyancy. *Wärme-Stoffübertrag.* **16** (1), 15–21.
MORTON, B.R. 1962 Coaxial turbulent jets. *Intl J. Heat Mass Transfer* **5** (10), 955–965.
MORTON, B.R. 1959 Forced plumes. *J. Fluid Mech.* **5** (1), 151–163.
MORTON, B.R., TAYLOR, G.I. & TURNER, J.S. 1956 Turbulent gravitational convection from maintained and instantaneous sources. *Proc. R. Soc. Lond.* A **234** (1196), 1–23.
PANCHAPAKESAN, N.R. & LUMLEY, J.L. 1993 Turbulence measurements in axisymmetric jets of air and helium. Part 1. Air jet. *J. Fluid Mech.* **246**, 197–223.
PAPANICOLAOU, P.N. & LIST, E.J. 1988 Investigations of round vertical turbulent buoyant jets. *J. Fluid Mech.* **195**, 341–391.
PINCINCE, A.B. & LIST, E.J. 1973 Disposal of brine into an estuary. *Journal (Water Pollution Control Federation)* **1**, 2335–2344.
PRIESTLEY, C.H.B. & BALL, F.K. 1955 Continuous convection from an isolated source of heat. *Q. J. R. Meteorol. Soc.* **81** (348), 144–157.
VAN REEUWIJK, M. & CRASKE, J. 2015 Energy-consistent entrainment relations for jets and plumes. *J. Fluid Mech.* **782**, 333–355.
VAN REEUWIJK, M., SALIZZONI, P., HUNT, G.R. & CRASKE, J. 2016 Turbulent transport and entrainment in jets and plumes: a DNS study. *Phys. Rev. Fluids* **1** (7), 074301.
SHABBIR, A. & GEORGE, W.K. 1994 Experiments on a round turbulent buoyant plume. *J. Fluid Mech.* **275**, 1–32.
SHRINIVAS, A.B. & HUNT, G.R. 2014 Unconfined turbulent entrainment across density interfaces. *J. Fluid Mech.* **757**, 573–598.
TALLURU, K.M., ARMFIELD, S., WILLIAMSON, N., KIRKPATRICK, M.P. & MILTON-MCGURK, L. 2021 Turbulence structure of neutral and negatively buoyant jets. *J. Fluid Mech.* **909**, A14.
TURNER, J.S. 1966 Jets and plumes with negative or reversing buoyancy. *J. Fluid Mech.* **26** (4), 779–792.
VEJRAŽKA, J., ZEDNÍKOVÁ, M. & STANOVSKÝ, P. 2018 Experiments on breakup of bubbles in a turbulent flow. *AIChE J.* **64** (2), 740–757.
WANG, H. & LAW, A.W.-K. 2002 Second-order integral model for a round turbulent buoyant jet. *J. Fluid Mech.* **459**, 397–428.
WILLIAMSON, N., ARMFIELD, S.W. & LIN, W. 2011 Forced turbulent fountain flow behaviour. *J. Fluid Mech.* **671**, 535–558.